BUD23-TRMT112 mediates the chromosomal tethering of Borna disease virus and catalyzes the internal m^7G methylation in viral RNA

Garcia Bea Clarise Baluyot

Table of Contents

Abstract 5

Abbreviations 7

Introduction 13

Chromosomal tethering of viruses 14

Nuclear infection of orthobornaviruses 14

Borna disease virus large protein 15

Proximity-dependent biotinylation 16

Materials and Methods 18

Cell lines and viruses 19

Plasmid construction 19

Transfection 20

BioID2 assay 20

Immunoprecipitation 21

Western blotting 21

Immunofluorescence assay 22

RNase A digestion 22

Reverse transcription PCR 23

Quantitative reverse transcription PCR 23

Lentivirus-based shRNA knockdown 24

$NaBH_4$ reduction and aniline cleavage of RNA 24

Ribosomal RNA analysis 24

DIG-labeled RNA construction 25

Northern blotting 26

STRING analysis 26

Statistical analysis 27

Results 28

Proximity-dependent biotinylation identifies the host protein interactors of BoDV-1 L 29

TRMT112, together with MTase partner BUD23, interacts with BoDV-1 vRNPs 30

BUD23-TRMT112 binds to RdRp domain of BoDV-1 L 31

Prolonged knockdown of BUD23 leads to short-lived increase in BoDV-1 replication 32

BUD23-TRMT112 mediates the chromosomal tethering of BoDV-1 vRNPs 34

BUD23 methylates the internal m^7G in BoDV-1 gRNA 35

Discussion 38

Host protein interactors of BoDV-1 L 39

Host functions of BUD23-TRMT112 and newfound role in BoDV-1 infection 40

Chromosomal tethering of BoDV-1 vRNPs 40

Internal m^7G methylation in host and BoDV-1 RNAs 41

Conclusion 43

Acknowledgements 44

References 46

Tables 54

1. Host protein interactors of BoDV-1 P 54

2. Host protein interactors of BoDV-1 L 55

S1. DNA oligonucleotide sequences used for BioID2 constructs 60

S2. Primer sequences used for PCR and RT-qPCR 61

S3. Silencer Select siRNAs used for knockdown 64

S4. Antibodies used for protein-based experiments 65

S5. DNA oligonucleotide sequences used for shRNA lentiviral vector constructs 66

Figures 67

1. Nuclear infection of BoDV-1 67

2. Alignment of conserved motifs between BoDV-1 L and VSV L 68

3. Identification of host protein interactors of BoDV-1 L by proximity-dependent biotinylation 69

4. Functional enrichments within the network of host protein interactors of BoDV-1 L 70

5. Interaction of TRMT112 and MTase partner BUD23 with BoDV-1 vRNPs 71

6. Binding of BUD23-TRMT112 to RdRp domain of BoDV-1 L 72

7. Transient knockdown of BUD23-TRMT112 and effect on BoDV-1 replication 73

8. Prolonged knockdown of BUD23 and effect on BoDV-1 replication 74

9. Role of BUD23-TRMT112 in the chromosomal tethering of BoDV-1 vRNPs 75

10. MTase activity of BUD23 is indispensable in the chromosomal tethering process 76

11. Internal m^7G methylation of BUD23 in BoDV-1 gRNA 77

12. Summary 78

Figure Legends 79

Abstract

Persistent nuclear infection is an uncommon infection strategy among RNA viruses. However, Borna disease virus 1 (BoDV-1), a nonsegmented negative-strand RNA virus, maintains infection in the cell nucleus by forming spheroidal aggregates known as viral speckles of transcripts (vSPOTs) which consists of viral ribonucleoproteins (vRNPs), and by tethering these vRNPs onto the host chromosomes during mitosis. While the mechanism on how BoDV-1 maintains nuclear infection is still far from understood, host proteins have been shown to be critically involved in the process. Investigating the host-viral interactions may therefore provide a better insight in the nuclear infection strategy of BoDV-1. In this study, the host protein interactors of BoDV-1 large (L) protein, a key component of the vRNP, were determined by proximity-dependent biotinylation. As a result, 77 host proteins were identified to be interacting with BoDV-1 L, 59 of which localize in the nucleus. Among the host proteins, TRM112, a partner to several methyltransferases (MTases), was further characterized for a putative role in BoDV-1 infection. It was discovered that TRMT112 binds with BoDV-1 L at the RNA-dependent RNA polymerase domain, together with BUD23, an 18S rRNA MTase and 40S ribosomal maturation factor. BUD23-TRMT112 was also observed to associate peripherally with the vSPOTs in the nucleus.

While transient knockdown of BUD23-TRMT112 did not show an overall change in the BoDV-1 replication, in contrast, prolonged knockdown of BUD23 caused a short-lived increase which subsequently led to decrease in the viral replication, as well as decreased localization of viral proteins to vSPOTs. Consequently, BUD23-TRMT112 was discovered to mediate the tethering of BoDV-1 vRNPs to chromosomes during mitosis. The MTase activity of BUD23 was also found to be indispensable in the tethering process. Accordingly, BUD23 was demonstrated to catalyze the internal m^7G methylation in BoDV-1 gRNA. It is speculated

that the internal m^7G may alter the tertiary structure of the gRNA, which may then result in a tighter association of vRNPs to the chromosomes.

The newfound functions of BUD23-TRMT112 in BoDV-1 therefore highlights the role of host-viral interactions in the chromosomal tethering, and overall, in the nuclear infection strategy of BoDV-1. In addition, the discovery of the m^7G methylation of BUD23-TRMT112 in BoDV-1 gRNA demonstrates the emerging significance of RNA modifications in viral infections.

Abbreviations

°C	Degrees Celsius
293LTV	293 Lentivirus
agRNA	Antigenome RNA
ALKBH8	AlkB homolog 8, tRNA methyltransferase
ANOVA	Analysis of variance
AP	Alkaline phosphatase
BioID	Biotin identification
BioID2	Biotin identification 2
BoDV-1	Borna disease virus 1
BoDV-1 G	Borna disease virus 1 glycoprotein
BoDV-1 L	Borna disease virus 1 large protein
BoDV-1 M	Borna disease virus 1 matrix protein
BoDV-1 N	Borna disease virus 1 nucleoprotein
BoDV-1 P	Borna disease virus 1 phosphoprotein
BoDV-1 X	Borna disease virus 1 accessory protein
BUD23	BUD23 rRNA methyltransferase and ribosome maturation factor
Cap	Capping
CDC2	Cell division control protein 2 homolog
CDK1	Cyclin-dependent kinase 1
cDNA	Complementary DNA
cl	Cleaved
cm	Centimeter
CO_2	Carbon dioxide

Ct	Cycle threshold
CTD	C-terminal domain
Da	Dalton
DAPI	4',6-Diamidino-2-phenylindole
DIG	Digoxigenin
DMEM	Dulbecco's Modified Eagle Medium
DNA	Deoxyribonucleic acid
dpt	Days post-transduction
DROSHA	Drosha ribonuclease III
DTT	Dithiothreitol
ECL	Enhanced chemiluminescence
EDTA	Ethylenediaminetetraacetic acid
Emp	Empty
FBS	Fetal bovine serum
FDR	False discovery rate
Fig	Figure
g	Gram
GAPDH	Glyceraldehyde-3-phosphate dehydrogenase
GN	Gene name
GO	Gene ontology
gRNA	Genome RNA
H2A	Histone H2A
H2B	Histone H2B
HIV-1	Human immunodeficiency virus 1
HMGB1	High mobility group box 1

hr	Hour
HRP	Horseradish peroxidase
HS	High sensitivity
Hsc70	Heat shock cognate 71 kDa
Hsp70	Heat shock protein 70 kDa
HSPA8	Heat shock protein family A (Hsp70) member 8
IFA	Immunofluorescence assay
IgG	Immunoglobulin G
IP	Immunoprecipitation
kb	Kilobase
kDa	Kilodalton
KEGG	Kyoto encyclopedia of genes and genomes
KMT9	Lysine methyltransferase 9
KSHV	Kaposi's sarcoma-associated herpesvirus
LANA	Latency-associated nuclear antigen
LC-MS/MS	Liquid Chromatography with tandem mass spectrometry
M	Molar
m^7G	7-Methylguanosine
m^7GTP	7-Methylguanosine triphosphate
MAFFT	Multiple alignment using fast Fourier transform
MEM	Minimum essential medium
MERM1	Metastasis-related methyltransferase 1
METTL5	Methyltransferase 5, N6-adenosine
mg	Milligram
min	Minute

miRNA	MicroRNA
mJ	Millijoule
mL	Milliliter
mM	Millimolar
mm	Millimeter
MOPS	3-(N-morpholino)propanesulfonic acid)
mRNA	Messenger RNA
MT	Methyltransferase (domain)
MTase	Methyltransferase
$NaBH_4$	Sodium borohydride
NAC	NAM, ATAF1/2 and CUC
NaCl	Sodium chloride
NaOAc	Sodium acetate
NARF	Nuclear prelamin A recognition factor
NEAA	Non-essential amino acids
ng	Nanogram
NLS	Nuclear localization signal
ns	Not significant
OL	Oligodendrocytes
OS	Organism name
PBS	Phosphate-buffered saline
PBST	PBS with Tween 20
PCR	Polymerase chain reaction
PE	Protein existence
Pfam	Protein family

pH	Potential of hydrogen
Phe	Phenylalanine
PPI	Protein-protein interaction
pri-miRNA	Primary microRNA
PRNTase	Guanosine diphosphate polyribonucleotidyltransferase
PVDF	Polyvinylidene difluoride
qPCR	Quantitative PCR
RBMX	RNA binding motif protein X-linked
RdRp	RNA-dependent RNA polymerase
Red	Reduced
Res	Resistant
RIPA	Radioimmunoprecipitation assay
RNA	Ribonucleic acid
RNase A	Ribonuclease A
rRNA	Ribosomal RNA
RT-PCR	Reverse transcription PCR
RT-qPCR	Quantitative reverse transcription PCR
s	Second
SDS	Sodium dodecyl sulfate
SDS-PAGE	Sodium dodecyl sulfate-polyacrylamide gel electrophoresis
SEM	Standard error of mean
shBUD23	BUD23 shRNA
shRNA	Short hairpin RNA
shScramble	Scramble shRNA
siBUD23	BUD23 siRNA

siHMGB1	HMGB1 siRNA
siNT	Non-targeting siRNA
siRNA	Small interfering RNA
siTRMT112	TRMT112 siRNA
SSC	Saline-sodium citrate
STRING	Search tool for recurring instances of neighboring genes
SV	Sequence version
TBST	Tris-buffered saline with Tween 20
Tris-HCl	Tris hydrochloride
TRMT11	tRNA methyltransferase 11 homolog
TRMT112	tRNA methyltransferase activator subunit 11-2
tRNA	Transfer RNA
U	Units
ucl	Uncleaved
µg	Microgram
µL	Microliter
µM	Micromolar
Vpr	Viral protein R
vRNP	Viral ribonucleoprotein
vSPOT	Viral speckle of transcripts
VSV	Vesicular stomatitis virus
WBSCR22	Williams-Beuren syndrome chromosome region 22, rRNA methyltransferase and ribosome maturation factor
WT	Wild type
xg	Relative centrifugal force

Introduction

Chromosomal tethering of viruses

Viral infections are characterized by the immediate production and release of progeny virions, leading to severe disruption of cellular processes or even cell death. On the other hand, some viruses have been shown to persist indefinitely inside the cells. Such is the strategy of papillomaviruses, adenoviruses, and herpesviruses, collectively known as persistently-infecting DNA viruses [1-6].

One particular strategy that persistently-infecting DNA viruses have in common is to tether to their viral genome DNA onto the host chromosomes during mitosis, which enables the virus to persist to the succeeding generation of cells. Specifically, the viruses tether their viral genome DNA in the form of extrachromosomal circular plasmid or episome (except for adenoviruses), assisted by dedicated viral genome maintenance proteins which may also interact with the host proteins. For example, the latency-associated nuclear antigen (LANA) protein of Kaposi's sarcoma-associated herpesvirus (KSHV) tethers the viral episome by simultaneously binding to the terminal repeats of the episome and to histones H2A and H2B of the nucleosomes and other chromatin-associated proteins [4,7]. During the mitosis, the viral episomes are then segregated along with the chromosomes to the daughter cells, allowing the viral infection to persist to the next generation of cells.

Nuclear infection of orthobornaviruses

Coincidence or not, chromosomal tethering is also a strategy of orthobornaviruses which adopted a persistent infection in the cell nucleus. Orthobornaviruses (genus *Orthobornavirus*; family *Bornaviridae*) are a group of non-segmented, negative-strand RNA viruses causing fatal neurological diseases in animals, and in rare cases, humans (Fig. 1A) [8-12]. These viruses form spheroidal cage-like aggregates of viral ribonucleoproteins (vRNPs) in the nucleus, which consists of the large (L) protein functioning as the RNA-dependent RNA

polymerase (RdRp), the phosphoprotein (P) acting as the cofactor, and the nucleoproteins (N) encapsidating the viral genome RNA (gRNA) (Fig. 1B, 1C). As sites of viral replication and transcription, these aggregates are referred to as "viral speckles of transcripts" or vSPOTs [13,14]. The accessory (X) and matrix (M) proteins are also recruited to the vSPOTs to modulate the viral replication. At the onset of mitosis, the vSPOTs disintegrate and the vRNPs tether onto the condensing chromosomes. The tethered vRNPs are then segregated along with the chromosomes to the daughter cells, enabling the viral infection to persist to the next generation of cells [13].

Studies on Borna disease virus 1 (BoDV-1) as the prototype mammalian orthobornavirus had shed some light onto the role of host-viral interactions in the nuclear infection of orthobornaviruses. For example, CDK1-cyclin B1 was found to bind with BoDV-1 N leading to prolongation of the cell cycle progression [15]. RBMX, a spliceosome and chromatin-associated protein, also binds with BoDV-1 N and is requisite in preserving the vSPOT structure [16]. HSPA8, a member of the Hsp70 protein family, binds with BoDV-1 X and recruits the viral protein to the nucleus [17]. HMGB1, another chromatin-associated protein, interacts with BoDV-1 P and is involved in the chromosomal tethering of vRNPs [13]. Still, these examples only reveal the tip of the iceberg on how nuclear infection of BoDV-1 may require the interplay of viral and host proteins.

Borna disease virus large protein

The BoDV-1 L is a multifunctional protein which houses the conserved domains and motifs that are shared among the other L proteins of mononegaviruses (order *Mononegavirales*) (Fig. 2A) [18-20]. The domains in BoDV-1 L include the RdRp which functions for viral replication and transcription, the GDP polyribonucleotidyltransferase (PRNTase or Cap) which functions for viral mRNA capping, and the C-terminal domain. The methyltransferase (MT)

domain which functions for viral mRNA cap methylation, is oddly absent. Conserved motifs are then found within the domains, some of which are necessary for the enzymatic functions. Motif a in the RdRp domain represent the KEKE [hydrophobic] K motif which serves as the template recognition site, while motif b in the Cap domain represent the GxxT and HR motifs which function for guanosine nucleotide binding and covalent RNA attachment, respectively (Fig. 2B, 2C). Motifs A, B, C, and D can also be found in the RdRp domain, wherein motif C represents the QGDNQ motif serving as the catalytic site of the RdRp (Fig. 2B). Altogether, the domains and motifs provide the basis for the functions of BoDV-1 L that are integral in viral infection. It is likely then that BoDV-1 L might interact with the host proteins to aid in its functions and in the nuclear infection of BoDV-1, which warrants further exploration.

.

Proximity-dependent biotinylation

Proximity-dependent biotinylation has been gaining attention as a method to identify protein-protein interactions (PPIs) in host-viral interaction studies [21,22]. This method utilizes the biotin ligase BirA from *Escherichia coli*, which specifically biotinylates acetyl coenzyme A carboxylase by forming an amide bond between the biotin and the lysine residue of the protein. The BirA is then humanized and rendered "promiscuous" by R118G amino acid substitution, termed as BioID, which allows for lesser specificity and affinity to the substrates. Consequently, the BioID is able to biotinylate proteins indiscriminately within a range of 10 nm. If fused to a bait protein of interest, the BioID will then be able to biotinylate and label proteins that are not just tightly bound, but also transiently interacting with the bait protein [23]. Therefore, proximity-dependent biotinylation by BioID has brought a novel approach to the identification of PPIs. Other advantages of this method include the capability to utilize stringent buffers and to omit the use of antibodies, all of which would have been difficult with the standard affinity purification [21,22]. Newer versions of BioID have also been constructed for

a smaller, more efficient, and temporally-controlled biotinylation, which have provided further improvements to the identification of PPIs [24-26].

In this study, the host protein interactors of BoDV-1 L were determined by proximity-dependent biotinylation. Among the host proteins, TRMT112, a partner of several MTases, was further characterized for a putative role in BoDV-1 infection. It was then found that TRMT112, together with BUD23, binds with BoDV-1 L specifically at the RdRp domain, and associates peripherally with the vSPOTs in the nucleus. BUD23, also known as WBSCR22 or MERM1, is an 18S rRNA MTase and a 40S ribosomal maturation factor [27-29]. While transient knockdown of BUD23-TRMT112 did not significantly affect the viral replication, in contrast, prolonged knockdown of BUD23 led to a short-lived increase and eventual decrease in the viral replication. It was then discovered that BUD23-TRMT112 mediates the tethering of BoDV-1 vRNPs to mitotic chromosomes, and that the MTase activity of BUD23 is necessary in the tethering process. In addition, BUD23 was demonstrated to methylate the internal m^7G in BoDV-1 gRNA. These newly discovered functions of BUD23-TRMT112 in BoDV-1 therefore demonstrate how host-viral interactions play critical roles in the chromosomal tethering and in the nuclear infection of orthobornaviruses.

Materials and Methods

Cell lines and viruses

Human oligodendrocytes (OL), which are persistently infected with BoDV-1 strain He/80/Fct (He/80/FR harboring a nucleotide substitution C4673T), were cultured in high-glucose (4.5%) DMEM supplemented with 5% FBS and 100 μg/mL penicillin-streptomycin. Human embryonic kidney 293LTV (293LTV) cells, which are also persistently-infected with the same BoDV-1 strain, were cultured in high-glucose DMEM supplemented with 10% FBS, 1X MEM NEAA, and 100 μg/mL penicillin-streptomycin. Both cell lines were maintained in a humidified atmosphere containing 5% CO_2 at 37°C.

Plasmid construction

BioID2 expression vector (pCAGGS-Myc-BioID2) was constructed by ligating double-stranded oligonucleotide encoding Myc-BioID2 sequence to linearized pCAGGS plasmid using DNA Ligation Kit, Mighty Mix (Takara). BioID2-L expression vector (pCAGGS-Myc-linker-BoDV-1 L) was then constructed by fusing single-stranded oligonucleotide encoding the (GGGS)3x linker sequence and PCR-amplified BoDV-1 L to linearized BioID2 expression vector using NEBuilder HiFi DNA Assembly Cloning Kit (NEB). Expression vectors encoding the host factors TRMT112, BUD23, ALKBH8, METLL5, KMT9, and TRMT11 were constructed by fusing PCR-amplified coding sequences with N-terminal Myc tag sequence to linearized pCAGGS plasmid using NEBuilder. For the expression vectors encoding BoDV-1 L domain truncations, corresponding segments encoding the sequences for RdRp (1-2343), Cap (2344-3705), CTD (3706-5133), RdRp-Cap (1-3705), and Cap-CTD (2344-5133) were PCR-amplified from pCAGGS-FLAG-BoDV-1 L with N-terminal FLAG tag sequence and fused to linearized pCAGGS plasmids using NEBuilder. For the expression vector encoding siRNA-resistant BUD23 named Res (pCAGGS-Myc-Res), two segments with nucleotide substitutions in the BUD23 coding sequence (A199T, G200C, T201A, A204T) were PCR-

amplified with N-terminal Myc tag sequence. The PCR-amplified segments were then fused to linearized pCAGGS plasmid using NEBuilder. From Res, MTase-defective BUD23 (pCAGGS-Myc-Res63) and TRMT112-binding-impaired (pCAGGS-Myc-Res117) were constructed by incorporating substitutions G188A and C189G for Res63 and A350C for Res117, using the same methods for Res. See also Table S1 for oligonucleotide sequences and Table S2 for primer sequences.

Transfection

Plasmids were transfected using polyethylenimine in 293LTV cells or Lipofectamine 2000 (Thermo Fisher Scientific) in OL cells. Silencer Select siRNAs (Table S3; Thermo Fisher Scientific) were transfected using Lipofectamine RNAiMAX (Thermo Fisher Scientific). For rescue experiments, siRNAs were transfected one day prior to plasmid transfection. Opti-MEM was used as the transfecting medium.

BioID2 assay

The following protocol was adapted from Cheah and Yamada [30] with some modifications. BoDV-1-infected 293LTV cells were seeded onto a 10-cm culture dish and were transfected with BioID2 or BioID2-L expression vector. One day post-transfection, the cells were fed with 50 μM biotin. Two days post-transfection, the cells were washed thrice with ice-cold PBS and lysed using 500 μL modified RIPA lysis buffer (150 mM NaCl, 50 mM Tris-HCl pH 7.4, 1 mM EDTA, 0.4% SDS, 1% Triton X-100, 1 mM DTT, 1X protease inhibitor cocktail) and 3 U benzonase for 30 min in 4°C with rotation. The lysates were sonicated for 2 min (30 s on/off) under high conditions and centrifuged at 12000 xg for 10 min in 4°C. The biotinylated proteins were then immunoprecipitated from the lysate supernatant using 500 μg Dynabeads MyOne Streptavidin T1 (Thermo Fisher Scientific) overnight in 4°C with rotation.

The beads were washed under ice-cold conditions: first with modified RIPA buffer, then with 2% SDS in 50 mM Tris-HCl pH 7.4, then twice more with modified RIPA buffer. Finally, the biotinylated proteins were eluted from the beads by boiling with 50 µL 1.3 mM biotin for 5 min in 95°C, after which 50 µL 2x sample buffer was added and was boiled for another 5 min. The immunoprecipitated proteins were visualized by SilverQuest Staining Kit (Thermo Fisher Scientific). The protein bands were then excised, digested in-gel with trypsin, and analyzed by Q Exactive Plus LC-MS/MS (Thermo Fisher Scientific). Proteins assigned to BioID2 and BioID2-L were then identified by protein matches and protein scores calculated by Mascot software (Matrix Science). Proteins with score of 50 ≤ from the difference of the scores between BioID2-P or BioID2-L and control BioID2 were then listed in Table 1 and 2, respectively, as bona fide host protein interactors.

Immunoprecipitation

Cells seeded to 10-cm dish were washed twice with ice-cold PBS and lysed using 500 µL IP buffer (150 mM NaCl, 20 mM Tris-HCl pH 7.4, 1 mM EDTA, 1% Triton X-100, 1x protease inhibitor cocktail) for 30 min in 4°C with rotation. Meanwhile, 1.5 mg Dynabeads Protein G (Dynabeads) were incubated with 3 µg antibody in IP buffer for 1 hr in 4°C with rotation. The lysates were then centrifuged at 12000 xg for 10 min in 4°C, after which the tagged proteins were immunoprecipitated from the lysate supernatant by mixing with the antibody-bead complex in IP buffer for 3 hr in 4°C with rotation. After incubation, the beads were washed thrice with ice-cold IP buffer, then transferred to new microfuge, and finally eluted with 1 µg/µL 3xFLAG (Thermo Fisher Scientific) or Myc (Thermo Fisher Scientific) peptide for 30 min in 37°C. Equal volume of 2x sample buffer was added, and the samples were boiled in 95°C for another 5 min. See also Table S4 for antibodies.

Western blotting

Cells were washed with PBS and resuspended in 1x sample buffer. The lysates were then boiled in 95°C for 10 min. Samples were run by SDS-PAGE and the separated proteins were transferred to PVDF membrane. The membrane was blocked with Blocking One (Nacalai Tesque) for 45 min and then with 5% skim milk in 0.05% Tween 20 in 1x Tris-buffered saline pH 7.4 (TBST) for another 45 min. The membrane was then incubated with the primary antibody diluted in Can Get Signal Solution 1 (Toyobo) for 1 hr or overnight in 4°C with gentle agitation. The membrane was washed with TBST for 30 min with gentle agitation, and then incubated with the HRP-conjugated secondary antibody diluted in Can Get Signal Solution 2 (Toyobo) for 1 hr with gentle agitation. The membrane was washed again with TBST for 30 min with gentle agitation, after which the membrane was viewed by chemiluminescence reaction using Clarity Max ECL Substrate (Bio-Rad) in Fusion Solo S (Vilber). See also Table S4 for antibodies.

Immunofluorescence assay

The cells were washed with PBS and fixed using 4% paraformaldehyde in PBS for 10 min. After fixation, the cells were washed twice with PBS and permeabilized using 0.1% Triton X-100 for 10 min. Following permeabilization, the cells were washed twice with PBS and then blocked using 10% goat serum in 0.05% Tween 20 in PBS (PBST). The cells were then incubated with primary antibodies diluted in 5% goat serum in PBST for 1 hr or overnight in 4°C. The cells were washed thrice with PBS and then incubated with secondary antibodies and DAPI diluted in 5% goat serum in PBST. Finally, the immunostained cells were washed thrice with PBS and viewed using Eclipse Ti confocal laser scanning microscope (Nikon) or EVOS M7000 Imaging system (Thermo Fisher Scientific). See also Table S4 for antibodies.

RNase A digestion

Cells seeded to 10-cm dish were washed twice with ice-cold PBS and lysed using 500 µL IP buffer (150 mM NaCl, 20 mM Tris-HCl pH 7.4, 1 mM EDTA, 1% Triton X-100, 1x protease inhibitor cocktail) added with 4, 40, or 400 mg RNase A (R6148, Sigma-Aldrich) for 30 min in 4°C with rotation. The digested RNA from cell lysate were purified by RNA Clean & Concentrator-25 (Zymo Research). The purified RNA was then loaded and run into Microchip Electrophoresis System-202 MultiNA (Shimadzu).

Reverse transcription PCR

To determine the RNAse A digestion in BoDV-1 gRNA, purified RNA was reverse-transcribed by Verso cDNA Synthesis Kit (Thermo Fisher Scientific) using BoDV-1 gRNA-specific primer. To amplify specific segments of the GAPDH mRNA, NARF mRNA, and BoDV-1 gRNA after $NaBH_4$/aniline treatment, purified RNA were reverse-transcribed by the same kit using oligo(dT) or BoDV-1 gRNA-specific primer.

The cDNA was then PCR-amplified using forward and reverse primers. See also Table S2 for primer sequences.

Quantitative reverse transcription PCR

Total RNA was reverse-transcribed by Verso cDNA Synthesis Kit using anchored oligo(dT), random hexamers, or BoDV-1 gRNA-specific primer. The cDNA was then amplified real-time by Luna Universal qPCR Master Mix (NEB) in Rotor-Gene Q (Qiagen), using forward and reverse. The threshold cycle (Ct) value was determined as the number of cycles at which a significant fluorescence increase was first detected. RNA expression levels were then quantified relative to GAPDH mRNA expression level, as recommended by Taylor et al. [31]. See also Table S2 for primer sequences.

Lentiviral shRNA knockdown

BUD23 shRNA target sequence was based from BUD23 siRNA, while Scramble shRNA target sequence was based from a scrambled sequence of BUD23 shRNA target sequence (Table S5). Lentiviral shRNA vectors, together with psPAX2 (Gag-Pro-Pol), and pMD2.G (VSV G) were then transfected to propagate lentiviruses in cell culture. Lentiviruses were then collected from cell supernatants, filtered through a 0.45 mm filter, and were transduced in BoDV-1-infected OL cells, wherein successfully-transduced cells were selected by puromycin.

$NaBH_4$ reduction and aniline cleavage of RNA

The following protocol was adapted from Pandolfini et al. [32] and Lin et al. [33] with some modifications. For one reaction, 4 μg total RNA was mixed with 7.4 mM m^7GTP and 1 M Tris-HCl pH 8.0 in final volume of 15 μL. For reduced conditions, freshly prepared 15 μL 1M $NaBH_4$ was added to the RNA and incubated for 40 min on ice, then 300 μL 0.75 mM NaOAc pH 5.2 with 20 μg glycogen was added to the mixture. For mock conditions, $NaBH_4$ was mixed with 300 μL 0.75 mM NaOAc pH 5.2 and boiled in 90°C for 30 min, then chilled on ice and added to RNA with 20 μg glycogen. The RNA was then purified by ethanol precipitation and resuspended in 19.2 μL RNase-free water. For cleavage of abasic sites following RNA reduction, the RNA was mixed with 8.2 μL acetic acid and 2.7 μL aniline (7:3:1 ratio) and incubated at room temperature for 2 hr under dark condition. The cleaved RNA was purified by another round of ethanol precipitation and resuspended in RNAse-free water. The purified RNA was quantified using Qubit RNA HS Assay Kit (Thermo Fisher Scientific).

Ribosomal RNA analysis

RNA samples were loaded and run into Microchip Electrophoresis System-202 MultiNA. After the run, the RNA amount associated to 28S (5.0 kb) and 18S rRNA (1.9 kb) peaks were used to calculate the 28S/18S rRNA ratio. For cleaved RNA, RNA amount associated to two cleaved (cl; 1.6 kb and 0.23 kb) and uncleaved (ucl; 1.9 kb) 18S rRNA peaks were used to calculate the cleaved/uncleaved ratio to determine the extent of 18S rRNA cleavage.

DIG-labeled RNA probe construction

The following protocol was adapted from DIG Application Manual for Filter Hybridization (Roche Applied Science). Total RNA were reverse-transcribed using SuperScript IV First-Strand Synthesis System (Thermo Fisher Scientific) Kit using oligo(dT) or BoDV-1 agRNA-specific primer. DIG-labeled probes for GAPDH mRNA, NARF mRNA, and BoDV-1 gRNA were then constructed using DIG RNA Labeling Kit (Roche Applied Science) using T7 RNA polymerase and PCR-amplified templates. The probes were purified using RNA Clean & Concentrator-5 (Zymo Research) and quantified using Qubit RNA HS Assay Kit. The probe yield were then estimated by first preparing serial dilutions of the DIG-labaled control RNA and the constructed probes, followed by spotting in positively-charged nylon membrane. The RNA were then crosslinked to membrane with 120 mJ using UVP CX-2000 UV Crosslinker (Analytik Jena). The membrane was then incubated with gentle agitation in the following buffers: washing buffer (Roche Applied Science) for 2 min, blocking buffer (Roche Applied Science) for 30 min, anti-Digoxigenin-AP antibody solution (Roche Applied Science) for 30 min, washing buffer twice for 15 min, and detection buffer (Roche Applied Science) for 3 min. The membrane was viewed by chemiluminescence reaction using CDP-Star Substrate (Thermo Fisher Scientific) in Fusion Solo S. See also Table S2 for primer sequences.

Northern blotting

Following $NaBH_4$/aniline-treatment, purified RNA were mixed with RNA sample loading buffer (R1386, Sigma-Aldrich). RNA samples were then denatured in 65°C for 10 min and immediately chilled on ice. RNA samples and DynaMarker Prestain Marker for RNA High ladder (BioDynamics) were loaded in 0.8% agarose gel made with 1X MOPS buffer and 2% formaldehyde, and then run in excess 1X MOPS buffer for 135 min. The gel was soaked twice in 20X SSC for 15 min, and then sandwiched in a wet transfer stack overnight with excess 20X SSC for the transfer of RNA to positively-charged nylon membrane. The stack was disassembled the following day, and the RNA was crosslinked to the membrane with 120 mJ using UVP CX-2000 UV Crosslinker. The membrane were washed with RNase-free water, air-dried, and incubated with DIG Easy Hyb buffer (Roche Applied Science) for 30 min in 68°C with gentle agitation. The membrane was then incubated with DIG Easy Hyb buffer mixed with denatured probes (80 ng/mL buffer) overnight in 68°C with gentle agitation. Following probe hybridization, the membrane was incubated with gentle agitation in 2X SSC containing 0.1% SDS twice for 2 min, then in 0.1X SSC containing 0.1% SDS twice for 15 min in 68°C. The membrane was then incubated with gentle agitation in the following buffers: washing buffer for 2 min, blocking buffer for 1 hr, anti-Digoxigenin-AP antibody solution for 30 min, washing buffer twice for 15 min, and detection buffer for 3 min. The membrane was viewed by chemiluminescence reaction using CDP-Star Substrate in Fusion Solo S.

STRING analysis

The list of proteins were imported to STRING wherein the active interaction sources selected were experiments and databases [34]. Network edges are based on confidence with minimum score of 0.4, wherein line thickness indicate strength of data support. The nuclear

proteins were then identified by Gene Ontology (GO) Cellular Component analysis (GO:0005634). Among the functional enrichments in the interaction network, top four protein family (Pfam) domains and top eight Kyoto Encyclopedia of Genes and Genomes (KEGG) pathways were exported according to calculated false discovery rate (FDR).

Statistical analysis

Significant differences between data sets were determined using GraphPad Prism version 9 (GraphPad Software Inc.). For two data sets, two-tailed t-test was used. For three or more data sets, two-tailed one-way ANOVA were used, followed by Dunnett's, Tukey's, or Šidák's multiple comparisons test as recommended by the software.

Results

Proximity-dependent biotinylation identifies the host protein interactors of BoDV-1 L

Proximity-dependent biotinylation was utilized to determine the host proteins interacting with BoDV-1 L, as well as with BoDV-1 P, which may be important in the nuclear infection of BoDV-1. First, a smaller engineered biotin ligase from *A. aeolicus*, termed as BioID2, was fused to the N-terminal region of the viral proteins with a Myc tag to form the recombinant proteins BioID2-L and BioID2-P, respectively (Fig. 3A) [25]. In the case of BioID2-L, a (GGGS)3x linker was attached between the BioID2 and BoDV-1 L to allow more flexibility of movement and wider biotinylation range to BioID2, against the larger BoDV-1 L. The BioID2 is then expected to biotinylate proteins that are bound and transiently interacting with the viral proteins in the presence of excess biotin (Fig. 3B). The localizations of the BioID2 recombinant proteins were also checked to ascertain that the proteins are located in their true environment. As observed in Fig. 3C, both BioID2-P and BioID2-L localize in the vSPOTs in the nucleus of BoDV-1-infected OL cells, while BioID2 does not. This finding assures that BioID2-P and BioID2-L will likely interact with bona-fide host protein interactors. In addition, this finding also confirms that BioID2 does not hamper with the proper localization of the recombinant proteins.

Next, proximity-dependent biotinylation assay was performed wherein excess biotin were fed to BoDV-1-infected 293LTV cells, one day post-transfection of the BioID2 recombinant plasmids. The biotinylated proteins were immunoprecipiated using streptavidin beads and were viewed by silver staining (Fig. 3D). Unique banding patterns were observed between the samples, indicating differently biotinylated proteins by the BioID2 recombinant proteins. Expectedly, the BioID2 recombinant proteins were also biotinylated in the process (Fig. 3D, asterisks). The proteins were then analyzed by mass spectrometry, after which the bona fide host protein interactors of BioID2-P and BioID2-L were determined by a cutoff score difference of 50≤ from the BioID2. The lists of host proteins were then inputted to STRING in

order to identify PPIs and other functional interactions [34]. As shown in Fig. 3E and 3F, six host proteins were identified to be interacting with BoDV-1 P, including HMGB1, which was also previously identified to be interacting with P [13,35]. This finding demonstrates that BioID2 indeed may have identified bona fide host protein interactors.

On the other hand, 77 host proteins were identified to be interacting with BoDV-1 L (Fig. 3G). In particular, there was a significant enrichment of PPI within the host protein network of BoDV-1 L, with a *p* value of < 1.0e-16 as calculated by STRING. Of the host proteins, 59 were assessed to localize in the nucleus by GO Cellular Component, with FDR value of 2.73e-11. There were also protein functions enriched within the host protein network. The top enriched Pfam domains include Hsp70 protein, Staufen C-terminal domain, NAC domain, and 14-3-3- proteins (Fig. 4A). Meanwhile, the top KEGG pathways include Epstein-Barr virus infection, protein-processing in the endoplasmic reticulum, legionellosis, and Influenza A (Fig. 4B). Overall, proximity-dependent biotinylation by BioID2 successfully identified the host protein interactors of BoDV-1 L which could play important roles in the nuclear infection of BoDV-1.

TRMT112 with MTase partner BUD23, interacts with BoDV-1 vRNPs

Among the host protein interactors of BoDV-1 L, TRMT112 was further characterized for a possible role in BoDV-1 infection. Notably, TRMT112 is a partner and co-activator of several MTases, including ALKBH8, BUD23, KMT9, METTL5, and TRMT11 [36-39]. TRMT112 has no function by itself, however, and so it is speculated that TRMT112 may be bound to one of these MTases while interacting with BoDV-1 L.

As shown in Fig. 5A, TRMT112 and one of its MTase partner, BUD23, co-immunoprecipitated with FLAG-BoDV-1 L in BoDV-1-infected 293LTV cells. Myc-tagged TRMT112 and BUD23 were also occasionally observed to localize in the periphery of vSPOTs

in the nucleus of BoDV-1-infected OL cells (Fig. 5B, arrows), unlike other Myc-tagged MTase partners of TRMT112 (Fig. 5C). To further support this observation, the localizations of endogenous TRMT112 and BUD23 were also examined. In congruence to previous studies, endogenous TRMT112 and BUD23 were observed to localize in the nucleus, while BUD23 was also observed to localize in the nucleoli, in both BoDV-1-infected OL and 293LTV cells (Fig. 4D) [38,40]. And similar to observations with Myc-tagged TRMT112 and BUD23, some aggregates of endogenous TRMT112 and BUD23 were observed to localize peripherally with the vSPOTs in the nucleus of infected cells (Fig. 5D, arrows). Altogether, these findings indicate that TRMT112 is interacting with BoDV-1 L, together with its MTase partner BUD23.

BUD23, also known as MERM1 or WBSCR22, is an 18S rRNA MTase. Aside from methylation, BUD23 also aids in the processing of 18S rRNA and in the maturation to 40S ribosomal factor [27,28,41]. TRMT112 then binds to BUD23 to stabilize the protein [38]. It is therefore curious how the interaction between BUD23-TRMT112 and BoDV-1 L may support the nuclear infection of BoDV-1.

BUD23-TRMT112 binds to RdRp domain of BoDV-1 L

Given that BoDV-1 L is part of the vRNP, it is likely that BUD23-TRMT112 may also be interacting with BoDV-1 L in the context of vRNPs. The interaction of BUD23-TRMT112 to BoDV-1 L upon dissociation of vRNPs was therefore investigated. Prior to immunoprecipitation, BoDV-1-infected 293LTV cell lysates were treated with RNase A to digest the gRNA and to consequently dissociate the vRNPs. Expectedly, the total RNA and BoDV-1 gRNA showed increased RNA digestion with increased RNase A treatment (Fig. 6A). However, the amount of immunoprecipitated FLAG-BoDV-1 L also decreased following the increased RNase A treatment (Fig. 6B). This may be attributed to the dissociation of vRNPs resulting to the decrease in the immunoprecipitated vRNPs. Notably, the latter was also

reflected by the decrease in the co-immunoprecipitation of BoDV-1 N and BoDV-1 P. Still, BUD23-TRMT112 were co-immunoprecipitated with FLAG-BoDV-1 L after vRNP dissociation (Fig. 6B). Corroborating this finding, BUD23-TRMT112 were also co-immunoprecipitated with FLAG-BoDV-1 L in non-infected 293LTV cell lysates (Fig. 6C). Therefore, these findings suggest that BUD23-TRMT112 can bind to BoDV-1 L adequately, and without the need of viral cofactors such as BoDV-1 P.

Next, the functional domain of BoDV-1 L to which BUD23-TRMT112 binds onto was further explored. To this end, BoDV-1 L domain truncations with N-terminal FLAG were constructed and were then checked for their localizations in non-infected OL cells (Fig. 6D, 6E). BoDV-1 L were observed to localize in the cytoplasm, and surprisingly, also forms aggregates in the nucleus. This may be attributed to the inherent nuclear localization signal (NLS) of BoDV-1 L that is located in the CTD. Expectedly, CTD were also observed to localize in the cytoplasm and in the nucleus. On the other hand, RdRp, Cap, RdRp-Cap, and Cap-CTD were observed to localize in the cytoplasm. Curiously, RdRp and RdRp-Cap were also observed to localize occasionally in the nucleoli, where BUD23 is also located. And as shown in Fig. 6F, BUD23-TRMT112 also co-immunoprecipitated with RdRp and RdRp-Cap. Therefore, these findings indicate that BUD23-TRMT112 specifically binds to the RdRp domain of BoDV-1 L. Given that RdRp functions for viral replication and transcription, these findings also suggest that BUD23-TRMT112 may participate in these viral processes.

Prolonged knockdown of BUD23 leads to short-lived increase in BoDV-1 replication

To determine the effect of BUD23-TRMT12 in BoDV-1 replication or transcription, siRNA-induced knockdown of both proteins were performed in BoDV-1-infected OL cells. As shown in Fig. 7A, the knockdowns led to the decrease in BUD23 and TRMT112 expression, moreover, TRMT112 knockdown also led to a slight decrease in BUD23 expression. As

previously mentioned, TRMT112 binds with BUD23 to stabilize the protein, hence the loss of TRMT112 may have led an increase in BUD23 degradation [38]. The effects of BUD23-TRMT112 knockdown in cell physiology were also examined. While others studies have reported that BUD23 knockdown resulted to significant decrease in cell proliferation, in this study, BUD23-TRMT112 knockdown did not significantly affect the proliferation of BoDV-1-infected OL cells (Fig. 7B) [29,42,43]. This finding therefore allows us to directly correlate the effects of BUD23-TRMT112 knockdown in viral infection. Expectedly, BUD23-TRMT112 knockdown also led to a significant decrease in the 18S rRNA level, hence, a significant increase in the 28S/18S rRNA ratio (Fig. 7C, 7D). While these findings reflect the loss of 18S rRNA processing after knockdown, these also suggest that 18S rRNA processing does not necessarily affect the cell proliferation.

On the other hand, BUD23-TRMT112 knockdown did not affect the BoDV-1 N and BoDV-1 P protein expression (Fig. 7A). In contrast, there was an observed increase in the BoDV-1 mRNA expression, although excluding the BoDV-1 gRNA (Fig. 7E). To further delve into this observation, prolonged BUD23 knockdown was performed by shRNA lentiviral system in BoDV-1-infected OL cells (Fig. 8A). Corroborating the observations in siRNA knockdown, there was an increase in the BoDV-1 replication at 16 dpt, as demonstrated by the observed increases in the BoDV-1 protein, mRNA, and gRNA expressions (Fig. 8A, 8B). Accordingly, there was also an increase in the BoDV-1 infection rate (Fig. 8C). This was, however, short-lived as drastic decrease was observed in the BoDV-1 replication at 29 dpt (Fig. 8A, 8B, 8C). Meanwhile, the vSPOTs appeared to be less distinct at 16 and 29 dpt, as manifested by a more cytoplasmic localization of the viral proteins, especially of BoDV-1 N (Fig. 8D). Therefore, the prolonged BUD23 knockdown may have caused the decrease in the localization of viral proteins to vSPOTs, which may then have eventually led to the decrease in the viral replication.

Remarkably, these findings resemble the observed effects of prolonged HMGB1 knockdown which led to the decrease in the BoDV-1 replication [13]. Notably, the HMGB1 knockdown also led to the decrease in the tethering of BoDV-1 vRNPs to chromosomes during mitosis. It can be inferred therefore that BUD23-TRMT112 may also function in the chromosomal tethering process.

BUD23-TRMT112 mediates the chromosomal tethering of BoDV-1 vRNPs

During mitosis, BoDV-1 vRNPs tether and segregate along with the chromosomes to the daughter cells, allowing the viral infection to persist indefinitely (Fig. 1C) [13,14]. There are instances, however, where vRNPs are observed to be not tethered to the mitotic chromosomes (Fig. 9A). And as shown in Fig. 8B, BUD23-TRMT112 knockdown led to the decrease in the amount of tethered vRNPs to chromosomes during mitosis, and interestingly, of the same level with HMGB1 knockdown (Fig. 9B). This finding confirms that BUD23-TRMT112 is indeed involved in the chromosomal tethering of BoDV-1 vRNPs. The possibility in which BUD23-TRMT112 and HMGB1 may cofunction in the chromosomal tethering process was also examined. As shown in Fig. 9C and 9D, BUD23-TRMT112 knockdown did not affect the HMGB1 expression nor its localization inside the vSPOTs, respectively. In addition, HMGB1 knockdown did not affect the BUD23 and TRMT112 expression (Fig. 9E). Therefore, these findings demonstrate that BUD23-TRMT112 and HMGB1 may instead be working independently in their function for the chromosomal tethering of BoDV-1 vRNPs.

BUD23, as an 18S rRNA MTase, specifically methylates the m^7G of the G1639 within the 18S rRNA [27,28]. Accordingly, the role of methylation activity by BUD23 in the chromosomal tethering of vRNPs was further investigated. As shown in Fig. 10A, BUD23 houses the MTase domain at the N-terminal region while the NLS is located at the C-terminal region [38,44,45]. Myc-tagged siRNA-resistant BUD23, named Res, was then constructed to

be expressed during the BUD23 knockdown. From Res, Res63 which is MTase-defective, and Res117 which is TRMT112-binding impaired, were constructed by G63E and D117A amino acid substitutions, respectively [27,38]. The loss of MTase activity of BUD23 variant Res63 was then examined by determining the effect on the m^7G1639 methylation level of 18S rRNA. To measure the m^7G methylation within the RNA, $NaBH_4$/aniline treatment was employed which cleaves the RNA specifically at the m^7G sites (Fig. 11A, 11B, 10B) [27,32,33]. Expectedly, the 1.9 kb 18S rRNA was cleaved resulting to 1.6 kb and 0.23 kb bands. The BUD23 variant Res was then able to rescue the methylation level in 18S rRNA, demonstrated by a lower cleavage ratio. On the other hand, Res63 was not able to rescue the methylation level in 18S rRNA as much as Res, indicating the loss of MTase activity of Res63. Next, the impairment of TRMT112-binding to BUD23 variant Res117 was also examined. As shown in Fig. 10C, TRMT112 was not able to co-immunoprecipitate with Res117, indicating the loss of binding to TRMT112 of Res117.

The rescue experiments were then performed by transfection of BUD23 Res variants in BUD23 siRNA-induced knockdown OL cells. As shown in Fig. 10D, expression of BUD23 variant Res resulted to an increase in tethered vRNPs to mitotic chromosomes. However, expression of BUD23 variants Res63 and Res117 did not result to increase in tethered vRNPs as observed with Res, indicating that the MTase activity and TRMT112-binding of BUD23 might play important roles in the chromosomal tethering process.

BUD23 methylates the internal m^7G in BoDV-1 gRNA

Given that the MTase activity of BUD23 is important in the chromosomal tethering of BoDV-1 vRNPs, the possibility of BUD23 methylation in BoDV-1 gRNA was also investigated. To determine the internal m^7G methylation in RNA, $NaBH_4$/aniline treatment was employed similarly in the previous experiment (Fig. 11A, 10B). In this method, $NaBH_4$

specifically reduces the m^7G in RNA, resulting to the loss of nucleobase in the sites. Consequently, the aniline then cleaves these abasic sites. As proof of mechanism, the 1.9 kb 18S rRNA was cleaved to 1.6 kb and 0.23 kb bands only after aniline treatment and under reducing conditions (Fig. 11B).

Some populations of tRNA, miRNA and mRNA have also been demonstrated to contain internal m^7G [32,33,46,47]. Particularly, the first study probing the internal m^7G methylation in mRNAs has identified transcripts containing m^7G and the specific methylation sites [46]. Among the mRNAs, the canonical NARF transcript, which contains m^7G1073, was used in this study as a positive control, while GAPDH transcript was used as negative control. Cleavage of BoDV-1 gRNA, NARF mRNA, and GAPDH mRNA, followed by Northern blotting and RT-PCR, would therefore identify the m^7G within these RNA. For Northern blotting, a DIG-labeled RNA probe was constructed to detect each RNA, while segments were amplified and detected by RT-PCR (Fig. 11C).

As shown in Fig. 11D, the 3.8 kb NARF mRNA was cleaved to 2.8 and 1.0 kb segments, with the probe detecting the latter segment. The cleavage can also be observed by RT-PCR, wherein the segment encompassing the m^7G site was also not amplified (Fig. 11E). Expectedly, GAPDH was not cleaved, indicating the m^7G-site specific cleavage of the $NaBH_4$/aniline treatment. On the other hand, BoDV-1 gRNA appeared to be cleaved as well, with the probe detecting a slightly lower band from the 8.9 kb gRNA band (Fig. 11F). There was also an observed decrease in the amplification of segments, especially at the 5'-leader end, by RT-PCR (Fig. 11G). These findings suggest that the BoDV-1 gRNA may contain at least an m^7G site near the 5'-leader end, although there is a possibility of more sites existing due to overall decreased band intensities by Northern blotting and RT-PCR. And as shown in Fig. 10H and 10I, the cleavage near the 5'-leader end of BoDV-1 gRNA decreased with BUD23 siRNA-

induced knockdown. Therefore, this finding indicates that BUD23 methylates the m^7G site near the 5-leader end of BoDV-1 gRNA.

Discussion

Host protein interactors of BoDV-1 L

In this study, the host protein interactors of BoDV-1 L were identified by proximity-dependent biotinylation using BioID2. As a result, 77 host proteins were identified to be interacting with BoDV-1 L, 59 of which were determined to be localizing in the nucleus. Interestingly, two of the host proteins were also previously reported to interact with the other BoDV-1 proteins. First is HSPA8 (also known as Hsc70), an Hsp70 protein family member. HSPA8 binds with BoDV-1 X and regulates the recruitment of the viral protein to the nucleus, thereby affecting the viral replication [17]. Second is CDK1 (also known as CDC2), wherein CDK-cyclin B1 binds with BoDV-1 N, which delays the G2-to-M phase transition, leading to cell cycle prolongation [15]. It is likely then that the host proteins identified in this study could also be interacting with the other viral proteins independently, or could be interacting with BoDV-1 L as part of the vRNPs.

Some of the host protein interactors of BoDV-1 L also belonged to Pfam of similar domains. The most enriched Pfam is the Hsp70 protein family, which has been implicated in the viral processes of several DNA and RNA viruses [48]. Hsp70 also co-purifies with the L-P polymerase complex of respiratory syncytial virus and Ebola virus and may exert a positive effect in the viral RNA synthesis [49-51]. Another Pfam, the 14-3-3 protein family, is primarily involved in the cell cycle regulation [52,53]. It was reported that the Vpr protein of human immunodeficiency virus 1 (HIV-1) binds with the 14-3-3 proteins, resulting to arrest in the G2-to-M phase transition [54]. On the other hand, Zika virus and Dengue virus interact with the 14-3-3 proteins to suppress the antiviral immunity [55,56]. Other Pfams, such as the Staufen C-terminal domain, was reported to interact with the HIV-1 for viral encapsidation, while the NAC domain was found to associate with the Hepatitis B virus [57-59]. Therefore, it will not be surprising if these Pfam domains may also play roles in the BoDV-1 infection

On the other hand, the most enriched KEGG pathways include the Epstein-Barr virus

infection and Influenza A. Interestingly, both viruses were known to infect the nucleus. This further supports that the host proteins interacting with BoDV-1 L may be involved in the nuclear infection of BoDV-1.

Host functions of BUD23-TRMT112 and newfound role in BoDV-1 infection

Among the host proteins, TRMT112, a partner and co-activator of several MTases, was further characterized for a putative role in BoDV-1 function. It was then discovered that TRMT112, together with BUD23, interacts at the RdRp domain of BoDV-1 L. BUD23 was first characterized as one of the genes deleted in chromosome 23 associated with Williams-Beuren syndrome [41]. Previous studies has also implicated BUD23 to cancer pathologies [44,60]. It was later discovered that BUD23 catalyzes the m^7G methylation in G1639 in 18S rRNA, and also influences the maturation of 40S ribosomal subunits independent of its methylation activity [27-29]. And in this study, it was found that BUD23-TRMT112 mediates the chromosomal tethering of BoDV-1 vRNPs, which may then affect the persistent infection of BoDV-1.

Chromosomal tethering of BoDV-1 vRNPs

HMGB1 is a non-histone chromatin-associated protein, which was also previously found to interact with BoDV-1 P and to colocalize in the vSPOTs. In addition, HMGB1 was found to be involved in the chromosomal tethering process [13]. It was speculated that the chromatin remodeling activity of HMGB1 may be important in fine-tuning the association of the tethered vRNPs onto the chromosomes via its interaction with BoDV-1 P. In this study, however, HMGB1 and BUD23-TRMT112 are working independently with their function in the chromosomal tethering of BoDV-1 vRNPs.

And so, as to how BUD23-TRMT112 exerts its role on the chromosomal tethering is still

unclear, but it can be speculate that the BUD23-TRMT112 might influence the chromatin architecture surrounding the vRNPs (Fig. 12). Aside from the ribosomal function, BUD23 also modulates the GR-mediated chromatin remodeling and GR-regulated histone modification [44]. It is worthy to note also that HMGB1 binds and associates to GR in the chromatin [61]. Therefore, it is plausible that BUD23 and HMGB1 may coordinate in mediating the chromosomal tethering of BoDV-1 vRNPs by remodeling the DNA architecture surrounding the vRNPs. Although the different localizations of BUD23-TRMT112 and HMGB1 with respect to vSPOTs make their interaction unlikely, the proteins may be recruited to function in different locations: HMGB1 might remodel the chromatin from inside the vSPOTs, while BUD23-TRMT112 might remodel the chromatin in the peripheral of the vSPOTs, resulting in a tighter association of vRNPs to chromosomes.

Internal m^7G methylation in BoDV-1 RNAs

On the other hand, the internal m^7G within the BoDV-1 gRNA catalyzed by BUD23-TRMT112 might indirectly influence the tethering of the vRNPs to the chromosomes (Fig. 12). Internal m^7G is an RNA modification that exists in 18S rRNA, as well as in some tRNA, mRNA, and miRNA species [27,32,33,46,47]. In addition, internal m^7G imparts a positive charge in the nucleobase which could influence the secondary or tertiary structure of the RNA. This phenomenon is particularly well-studied in yeast $tRNA^{Phe}$, wherein the m^7G46 at the variable loop strengthens the C13–G22-m^7G46 base triple interaction that is integral in maintaining the tRNA structure [62-64]. It was also observed that m^7G11 in *let-7-5p* miRNAs disrupts the Hoogsteen base-paired G-quadruplex structure within the pri-miRNA, thereby allowing the DROSHA to bind and process the pri-miRNA effectively [32]. Although the mechanism is still unclear, internal m^7G is also accumulated in some mRNA species under stress conditions, which may impart some stability and promote translation efficiency [47]. Therefore, it is

speculated that the m^7G sites may affect the encapsidation of the nucleoproteins or the overall structure of the vRNP. And these changes may then be essential in the tight association of the vRNPs to the chromosomes. Furthermore, the peripheral localization of BUD23-TRMT112 with respect to vSPOTs suggest that the methylation might occur during the viral replication, as it was previously reported that active replication sites may potentially be located at the outer edge of the vSPOTs. The specific binding of BUD23-TRMT112 to RdRp domain of BoDV-1 L may then assist the efficient methylation of newly-synthesizing gRNA.

Conclusion

The discovery of the viral functions of BUD23-TRMT112 in BoDV-1 has brought a new piece in understanding the mechanism behind the chromosomal tethering of BoDV-1, which suggests that chromosomal tethering is more than a simple mechanism and may require an interplay between the viral and host factors. Moreover, this study has uncovered several other host factors interacting with BoDV-1 L which may also likely play significant roles in the overall nuclear infection strategy of BoDV-1.

In addition, this study has demonstrated the presence of internal m^7G methylation in BoDV-1 gRNA, suggesting that this particular RNA modification has still much untapped potential for discovery for functions not just in host but also in viruses.

Acknowledgements

First, I give my heartfelt gratitude and appreciation to all the people who have supported me in this PhD endeavor, especially:

Dr. Keizo Tomonaga, for his kindness in accepting me to his laboratory, and for his support and patience despite my shortcomings;

Dr. Masayuki Horie, for his encouragements and invaluable advices which helped me gain confidence in self and research;

Shohei Kojima, Yahiro Mukai, Junna Kawasaki, Hsien-Hen Lin, and Koichi Kitao, for their constructive comments during the progress meetings;

Tomonaga lab members: Makino-sensei, Yamashita-san, Tanaka-san, Komorizono-san, Sakai-san, Kanda-san, Iwata-san, and former members Onimaru-chan, Watanabe-kun, Kim-kun, Yamamoto-san, and Kakuya-kun, for their small acts of kindness and assistance;

Nishimoto-san and the staff of the Student Affairs Section, for these years of warm assistance and accommodation with my student needs;

Mako-san, Mukai-kun, Johnson (Hsien-Hen), and Nabeka-kun, for the their steadfast moral support in difficult times;

Macky, Matthew, Francine, Faith, and the Kyoto Association of Pinoy Scholars, for keeping up the Filipino spirit of giving and camaraderie;

And to my family, Almario, Edna, Joan and Dean, for their enduring affection and concern on my well-being.

Second, I give my warm regards to *Yuzo Watanabe and Dr. Fuyuki Ishikawa* of the Laboratory of Cell Cycle Regulation for kindly performing the mass spectrometry analysis.

Third, I thank the *Monbukagakusho* for providing me the scholarship making my studies here in Japan possible. I also extend my gratitude to the *Kyoto University* and the *Association of Filipino Students in Japan* for the financial aids which helped me get through

the extension of study.

This thesis was supported in part by the JSPS KAKENHI grant numbers JP19K22530 (KT) and JP20H05682 (KT); MEXT KAKENHI grant numbers JP16H06429, JP16K21723, JP16H06430 (all to KT); JSPS Core-to-Core Program (KT); and the Joint Usage/Research Center Program on inFront, Kyoto University.

This thesis was based on a material contained in the following scholarly paper:

Authors: Garcia BCB, Horie M, Kojima S, Makino A, & Tomonaga K

Title: BUD23-TRMT112 interacts with the L protein of Borna disease virus and mediates the chromosomal tethering of viral ribonucleoproteins

Journal: Microbiology and Immunology, in press

References

1. Delecluse HJ, Bartnizke S, Hammerschmidt W, Bullerdiek J, Bornkamm GW (1993) Episomal and integrated copies of Epstein-Barr virus coexist in Burkitt lymphoma cell lines. J Virol 67: 1292-1299.

2. Lehman CW, Botchan MR (1998) Segregation of viral plasmids depends on tethering to chromosomes and is regulated by phosphorylation. Proc Natl Acad Sci U S A 95: 4338-4343.

3. Cotter MA, 2nd, Robertson ES (1999) The latency-associated nuclear antigen tethers the Kaposi's sarcoma-associated herpesvirus genome to host chromosomes in body cavity-based lymphoma cells. Virology 264: 254-264.

4. Aydin I, Schelhaas M (2016) Viral Genome Tethering to Host Cell Chromatin: Cause and Consequences. Traffic 17: 327-340.

5. Komatsu T, Quentin-Froignant C, Carlon-Andres I, Lagadec F, Rayne F, et al. (2018) In Vivo Labelling of Adenovirus DNA Identifies Chromatin Anchoring and Biphasic Genome Replication. J Virol 92.

6. Mauch-Mucke K, Schon K, Paulus C, Nevels MM (2020) Evidence for Tethering of Human Cytomegalovirus Genomes to Host Chromosomes. Front Cell Infect Microbiol 10: 577428.

7. Verma SC, Cai Q, Kreider E, Lu J, Robertson ES (2013) Comprehensive analysis of LANA interacting proteins essential for viral genome tethering and persistence. PLoS One 8: e74662.

8. Maes P, Amarasinghe GK, Ayllon MA, Basler CF, Bavari S, et al. (2019) Taxonomy of the order Mononegavirales: second update 2018. Arch Virol 164: 1233-1244.

9. Briese T, de la Torre JC, Lewis A, Ludwig H, Lipkin WI (1992) Borna disease virus, a negative-strand RNA virus, transcribes in the nucleus of infected cells. Proc Natl Acad Sci U S A 89: 11486-11489.

10. Niller HH, Angstwurm K, Rubbenstroth D, Schlottau K, Ebinger A, et al. (2020) Zoonotic spillover infections with Borna disease virus 1 leading to fatal human encephalitis, 1999-2019: an epidemiological investigation. Lancet Infect Dis 20: 467-477.

11. Kistler AL, Gancz A, Clubb S, Skewes-Cox P, Fischer K, et al. (2008) Recovery of divergent avian bornaviruses from cases of proventricular dilatation disease: identification of a candidate etiologic agent. Virol J 5: 88.

12. Hyndman TH, Shilton CM, Stenglein MD, Wellehan JFX, Jr. (2018) Divergent bornaviruses from Australian carpet pythons with neurological disease date the origin of extant Bornaviridae prior to the end-Cretaceous extinction. PLoS Pathog 14: e1006881.

13. Matsumoto Y, Hayashi Y, Omori H, Honda T, Daito T, et al. (2012) Bornavirus closely associates and segregates with host chromosomes to ensure persistent intranuclear infection. Cell Host Microbe 11: 492-503.

14. Hirai Y, Hirano Y, Matsuda A, Hiraoka Y, Honda T, et al. (2016) Borna Disease Virus Assembles Porous Cage-like Viral Factories in the Nucleus. J Biol Chem 291: 25789-25798.

15. Planz O, Pleschka S, Oesterle K, Berberich-Siebelt F, Ehrhardt C, et al. (2003) Borna disease virus nucleoprotein interacts with the CDC2-cyclin B1 complex. J Virol 77: 11186-11192.

16. Hirai Y, Honda T, Makino A, Watanabe Y, Tomonaga K (2015) X-linked RNA-binding motif protein (RBMX) is required for the maintenance of Borna disease virus nuclear viral factories. J Gen Virol 96: 3198-3203.

17. Hayashi Y, Horie M, Daito T, Honda T, Ikuta K, et al. (2009) Heat shock cognate protein 70 controls Borna disease virus replication via interaction with the viral non-structural protein X. Microbes Infect 11: 394-402.

18. Cubitt B, Oldstone C, de la Torre JC (1994) Sequence and genome organization of Borna disease virus. J Virol 68: 1382-1396.

19. Briese T, Schneemann A, Lewis AJ, Park YS, Kim S, et al. (1994) Genomic organization of Borna disease virus. Proc Natl Acad Sci U S A 91: 4362-4366.

20. Liang B, Li Z, Jenni S, Rahmeh AA, Morin BM, et al. (2015) Structure of the L Protein of Vesicular Stomatitis Virus from Electron Cryomicroscopy. Cell 162: 314-327.

21. Gillen J, Nita-Lazar A (2019) Experimental Analysis of Viral-Host Interactions. Front Physiol 10: 425.

22. Varnaite R, MacNeill SA (2016) Meet the neighbors: Mapping local protein interactomes by proximity-dependent labeling with BioID. Proteomics 16: 2503-2518.

23. Roux KJ, Kim DI, Raida M, Burke B (2012) A promiscuous biotin ligase fusion protein identifies proximal and interacting proteins in mammalian cells. J Cell Biol 196: 801-810.

24. Branon TC, Bosch JA, Sanchez AD, Udeshi ND, Svinkina T, et al. (2018) Efficient proximity labeling in living cells and organisms with TurboID. Nat Biotechnol 36: 880-887.

25. Kim DI, Jensen SC, Noble KA, Kc B, Roux KH, et al. (2016) An improved smaller biotin ligase for BioID proximity labeling. Mol Biol Cell 27: 1188-1196.

26. Trinkle-Mulcahy L (2019) Recent advances in proximity-based labeling methods for interactome mapping. F1000Res 8.

27. Haag S, Kretschmer J, Bohnsack MT (2015) WBSCR22/Merm1 is required for late nuclear pre-ribosomal RNA processing and mediates N7-methylation of G1639 in human 18S rRNA. RNA 21: 180-187.

28. White J, Li Z, Sardana R, Bujnicki JM, Marcotte EM, et al. (2008) Bud23 methylates G1575 of 18S rRNA and is required for efficient nuclear export of pre-40S subunits. Mol Cell Biol 28: 3151-3161.

29. Ounap K, Kasper L, Kurg A, Kurg R (2013) The human WBSCR22 protein is involved in the biogenesis of the 40S ribosomal subunits in mammalian cells. PLoS One 8: e75686.

30. Cheah JS, Yamada S (2017) A simple elution strategy for biotinylated proteins bound to streptavidin conjugated beads using excess biotin and heat. Biochem Biophys Res Commun 493: 1522-1527.

31. Taylor SC, Nadeau K, Abbasi M, Lachance C, Nguyen M, et al. (2019) The Ultimate qPCR Experiment: Producing Publication Quality, Reproducible Data the First Time. Trends Biotechnol 37: 761-774.

32. Pandolfini L, Barbieri I, Bannister AJ, Hendrick A, Andrews B, et al. (2019) METTL1 Promotes let-7 MicroRNA Processing via m7G Methylation. Mol Cell 74: 1278-1290 e1279.

33. Lin S, Liu Q, Lelyveld VS, Choe J, Szostak JW, et al. (2018) Mettl1/Wdr4-Mediated m(7)G tRNA Methylome Is Required for Normal mRNA Translation and Embryonic Stem Cell Self-Renewal and Differentiation. Mol Cell 71: 244-255 e245.

34. Szklarczyk D, Gable AL, Lyon D, Junge A, Wyder S, et al. (2019) STRING v11: protein-protein association networks with increased coverage, supporting functional discovery in genome-wide experimental datasets. Nucleic Acids Res 47: D607-D613.

35. Kamitani W, Shoya Y, Kobayashi T, Watanabe M, Lee BJ, et al. (2001) Borna disease virus phosphoprotein binds a neurite outgrowth factor, amphoterin/HMG-1. J Virol 75: 8742-8751.

36. Metzger E, Wang S, Urban S, Willmann D, Schmidt A, et al. (2019) KMT9 monomethylates histone H4 lysine 12 and controls proliferation of prostate cancer cells. Nat Struct Mol Biol 26: 361-371.

37. van Tran N, Ernst FGM, Hawley BR, Zorbas C, Ulryck N, et al. (2019) The human 18S rRNA m6A methyltransferase METTL5 is stabilized by TRMT112. Nucleic Acids Res 47: 7719-7733.

38. Ounap K, Leetsi L, Matsoo M, Kurg R (2015) The Stability of Ribosome Biogenesis Factor WBSCR22 Is Regulated by Interaction with TRMT112 via Ubiquitin-Proteasome Pathway. PLoS One 10: e0133841.

39. Fu D, Brophy JA, Chan CT, Atmore KA, Begley U, et al. (2010) Human AlkB homolog ABH8 Is a tRNA methyltransferase required for wobble uridine modification and DNA damage survival. Mol Cell Biol 30: 2449-2459.

40. Zorbas C, Nicolas E, Wacheul L, Huvelle E, Heurgue-Hamard V, et al. (2015) The human 18S rRNA base methyltransferases DIMT1L and WBSCR22-TRMT112 but not rRNA modification are required for ribosome biogenesis. Mol Biol Cell 26: 2080-2095.

41. Doll A, Grzeschik KH (2001) Characterization of two novel genes, WBSCR20 and WBSCR22, deleted in Williams-Beuren syndrome. Cytogenet Cell Genet 95: 20-27.

42. Baxter M, Voronkov M, Poolman T, Galli G, Pinali C, et al. (2020) Cardiac mitochondrial function depends on BUD23 mediated ribosome programming. Elife 9.

43. Yan D, Tu L, Yuan H, Fang J, Cheng L, et al. (2017) WBSCR22 confers oxaliplatin resistance in human colorectal cancer. Sci Rep 7: 15443.

44. Jangani M, Poolman TM, Matthews L, Yang N, Farrow SN, et al. (2014) The methyltransferase WBSCR22/Merm1 enhances glucocorticoid receptor function and is regulated in lung inflammation and cancer. J Biol Chem 289: 8931-8946.

45. Lyu G, Zong L, Zhang C, Huang X, Xie W, et al. (2019) Metastasis-related methyltransferase 1 (Merm1) represses the methyltransferase activity of Dnmt3a and facilitates RNA polymerase I transcriptional elongation. J Mol Cell Biol 11: 78-90.

46. Zhang LS, Liu C, Ma H, Dai Q, Sun HL, et al. (2019) Transcriptome-wide Mapping of Internal N(7)-Methylguanosine Methylome in Mammalian mRNA. Mol Cell 74: 1304-1316 e1308.

47. Malbec L, Zhang T, Chen YS, Zhang Y, Sun BF, et al. (2019) Dynamic methylome of internal mRNA N(7)-methylguanosine and its regulatory role in translation. Cell Res 29: 927-941.

48. Wan Q, Song D, Li H, He ML (2020) Stress proteins: the biological functions in virus infection, present and challenges for target-based antiviral drug development. Signal Transduct Target Ther 5: 125.

49. Noton SL, Deflube LR, Tremaglio CZ, Fearns R (2012) The respiratory syncytial virus polymerase has multiple RNA synthesis activities at the promoter. PLoS Pathog 8: e1002980.

50. Munday DC, Wu W, Smith N, Fix J, Noton SL, et al. (2015) Interactome analysis of the human respiratory syncytial virus RNA polymerase complex identifies protein

chaperones as important cofactors that promote L-protein stability and RNA synthesis. J Virol 89: 917-930.

51. Tchesnokov EP, Raeisimakiani P, Ngure M, Marchant D, Gotte M (2018) Recombinant RNA-Dependent RNA Polymerase Complex of Ebola Virus. Sci Rep 8: 3970.

52. Gardino AK, Yaffe MB (2011) 14-3-3 proteins as signaling integration points for cell cycle control and apoptosis. Semin Cell Dev Biol 22: 688-695.

53. Hermeking H, Benzinger A (2006) 14-3-3 proteins in cell cycle regulation. Semin Cancer Biol 16: 183-192.

54. Kino T, Gragerov A, Valentin A, Tsopanomihalou M, Ilyina-Gragerova G, et al. (2005) Vpr protein of human immunodeficiency virus type 1 binds to 14-3-3 proteins and facilitates complex formation with Cdc25C: implications for cell cycle arrest. J Virol 79: 2780-2787.

55. Chan YK, Gack MU (2016) A phosphomimetic-based mechanism of dengue virus to antagonize innate immunity. Nat Immunol 17: 523-530.

56. Riedl W, Acharya D, Lee JH, Liu G, Serman T, et al. (2019) Zika Virus NS3 Mimics a Cellular 14-3-3-Binding Motif to Antagonize RIG-I- and MDA5-Mediated Innate Immunity. Cell Host Microbe 26: 493-503 e496.

57. Li D, Wang XZ, Ding J, Yu JP (2005) NACA as a potential cellular target of hepatitis B virus preS1 protein. Dig Dis Sci 50: 1156-1160.

58. Banerjee A, Benjamin R, Balakrishnan K, Ghosh P, Banerjee S (2014) Human protein Staufen-2 promotes HIV-1 proliferation by positively regulating RNA export activity of viral protein Rev. Retrovirology 11: 18.

59. Mouland AJ, Mercier J, Luo M, Bernier L, DesGroseillers L, et al. (2000) The double-stranded RNA-binding protein Staufen is incorporated in human immunodeficiency

virus type 1: evidence for a role in genomic RNA encapsidation. J Virol 74: 5441-5451.

60. Nakazawa Y, Arai H, Fujita N (2011) The novel metastasis promoter Merm1/Wbscr22 enhances tumor cell survival in the vasculature by suppressing Zac1/p53-dependent apoptosis. Cancer Res 71: 1146-1155.

61. Agresti A, Scaffidi P, Riva A, Caiolfa VR, Bianchi ME (2005) GR and HMGB1 interact only within chromatin and influence each other's residence time. Mol Cell 18: 109-121.

62. Wintermeyer W, Zachau HG (1975) Tertiary structure interactions of 7-methylguanosine in yeast tRNA Phe as studied by borohydride reduction. FEBS Lett 58: 306-309.

63. Robertus JD, Ladner JE, Finch JT, Rhodes D, Brown RS, et al. (1974) Structure of yeast phenylalanine tRNA at 3 A resolution. Nature 250: 546-551.

64. Oliva R, Cavallo L, Tramontano A (2006) Accurate energies of hydrogen bonded nucleic acid base pairs and triplets in tRNA tertiary interactions. Nucleic Acids Res 34: 865-879.

Table 1. Host protein interactors of BoDV-1 P by proximity-dependent biotinylation.

Accession number	Description	Mass (Da)	BioID2 (A)			BioID2-P (B)			Score difference (B-A)
			Score	Matches	Sample number	Score	Matches	Sample number	
P09429	High mobility group protein B1 OS=Homo sapiens GN=HMGB1 PE=1 SV=3	24878	0	0	-	279	10	11	279
Q14247-2	Isoform 2 of Src substrate cortactin OS=Homo sapiens GN=CTTN	70915	0	0	-	226	5	5	226
P26583	High mobility group protein B2 OS=Homo sapiens GN=HMGB2 PE=1 SV=2	24019	0	0	-	133	5	11	133
X6RJP6	Transgelin-2 (Fragment) OS=Homo sapiens GN=TAGLN2 PE=1 SV=1	21073	0	0	-	98	2	12	98
H3BMT0	Jupiter microtubule-associated homolog 2 (Fragment) OS=Homo sapiens GN=JPT2 PE=1 SV=1	12223	94	2	12	162	3	12	68
G3V3A4	SNW domain-containing protein 1 OS=Homo sapiens GN=SNW1 PE=1 SV=1	65351	0	0	-	64	1	7	64

Table 2. Host protein interactors of BoDV-1 L by proximity-dependent biotinylation.

Accession number	Description	Mass (Da)	BioID2 (A)			BioID2-L (B)			Score difference (B-A)
			Score	Matches	Sample number	Score	Matches	Sample number	
A0A0G2JIW1	Heat shock 70 kDa protein 1B OS=Homo sapiens GN=HSPA1B PE=1 SV=1	70066	623	13	6	1937	110	6	1314
Q9UNZ2	NSFL1 cofactor p47 OS=Homo sapiens GN=NSFL1C PE=1 SV=2	40548	0	0	-	686	15	8	686
P54652	Heat shock-related 70 kDa protein 2 OS=Homo sapiens GN=HSPA2 PE=1 SV=1	69978	0	0	-	423	21	6	423
Q4VCS5	Angiomotin OS=Homo sapiens GN=AMOT PE=1 SV=1	118013	59	1	3	468	9	3	409
A0A087X1A5	Double-stranded RNA-binding protein Staufen homolog 1 OS=Homo sapiens GN=STAU1 PE=1 SV=1	54912	203	4	7	596	13	7	393
Q53FA3	HSPA1L (Fragment) OS=Homo sapiens GN=HSPA1L PE=1 SV=1	70360	0	0	-	369	8	5	369
O95817	BAG family molecular chaperone regulator 3 OS=Homo sapiens GN=BAG3 PE=1 SV=3	61557	0	0	-	312	9	5	312
Q9BWF3	RNA-binding protein 4 OS=Homo sapiens GN=RBM4 PE=1 SV=1	40289	0	0	-	310	5	9	310
Q9NZI8	Insulin-like growth factor 2 mRNA-binding protein 1 OS=Homo sapiens GN=IGF2BP1 PE=1 SV=2	63441	363	8	6	665	14	6	302
E9PKE3	Heat shock cognate 71 kDa protein OS=Homo sapiens GN=HSPA8 PE=1 SV=1	68763	178	4	6	453	24	6	275
P62258	14-3-3 protein epsilon OS=Homo sapiens GN=YWHAE PE=1 SV=1	29155	0	0	-	260	6	10	260
O43396	Thioredoxin-like protein 1 OS=Homo sapiens GN=TXNL1 PE=1 SV=3	32231	0	0	-	255	5	9	255
P25685	DnaJ homolog subfamily B member 1 OS=Homo sapiens GN=DNAJB1 PE=1 SV=4	38020	456	12	9	698	31	9	242
Q5JP53	Tubulin beta chain OS=Homo sapiens GN=TUBB PE=1 SV=1	47736	0	0	-	240	5	7	240
P17066	Heat shock 70 kDa protein 6 OS=Homo sapiens GN=HSPA6 PE=1 SV=2	70984	274	5	6	512	38	6	238
P20290	Transcription factor BTF3 OS=Homo sapiens GN=BTF3 PE=1 SV=1	22154	0	0	-	220	6	12	220

H0YHX9	Nascent polypeptide-associated complex subunit alpha (Fragment) OS=Homo sapiens GN=NACA PE=1 SV=1	22930	180	3	9	381	13	9	201
Q53EZ4	Centrosomal protein of 55 kDa OS=Homo sapiens GN=CEP55 PE=1 SV=3	54145	0	0	-	184	4	7	184
A0A1W2PQM2	Tubulin alpha-1C chain OS=Homo sapiens GN=TUBA1C PE=1 SV=1	36628	0	0	-	179	5	7	179
O95229	ZW10 interactor OS=Homo sapiens GN=ZWINT PE=1 SV=2	31274	0	0	-	177	3	9	177
P31689	DnaJ homolog subfamily A member 1 OS=Homo sapiens GN=DNAJA1 PE=1 SV=2	44839	0	0	-	176	4	8	176
A0A024QZP7	Cell division cycle 2, G1 to S and G2 to M, isoform CRA_a OS=Homo sapiens GN=CDC2 PE=1 SV=1	34060	0	0	-	158	4	10	158
P31947	14-3-3 protein sigma OS=Homo sapiens GN=SFN PE=1 SV=1	27757	0	0	-	145	4	10	145
Q04917	14-3-3 protein eta OS=Homo sapiens GN=YWHAH PE=1 SV=4	28201	0	0	-	145	4	10	145
P04792	Heat shock protein beta-1 OS=Homo sapiens GN=HSPB1 PE=1 SV=2	22768	0	0	-	129	3	11	129
A6NMY6	Putative annexin A2-like protein OS=Homo sapiens GN=ANXA2P2 PE=5 SV=2	38635	0	0	-	129	3	9	129
E9PL10	Transcription factor BTF3 OS=Homo sapiens GN=BTF3L4 PE=1 SV=1	15769	0	0	-	119	4	12	119
F5GX77	Multifunctional methyltransferase subunit TRM112-like protein OS=Homo sapiens GN=TRMT112 PE=1 SV=1	11964	0	0	-	115	2	14	115
H0YFC6	GTP-binding nuclear protein Ran (Fragment) OS=Homo sapiens GN=RAN PE=1 SV=1	11672	0	0	-	115	3	11	115
O60493	Sorting nexin-3 OS=Homo sapiens GN=SNX3 PE=1 SV=3	18751	0	0	-	113	3	13	113
Q9Y265	RuvB-like 1 OS=Homo sapiens GN=RUVBL1 PE=1 SV=1	50196	0	0	-	113	2	7	113
E9PJ81	UBX domain-containing protein 1 (Fragment) OS=Homo sapiens GN=UBXN1 PE=1 SV=1	32592	0	0	-	112	2	9	112
P60709	Actin, cytoplasmic 1 OS=Homo sapiens GN=ACTB PE=1 SV=1	41710	0	0	-	110	3	8	110
G3V4F7	Signal recognition particle 54 kDa protein OS=Homo sapiens GN=SRP54 PE=1 SV=1	48638	0	0	-	109	3	7	109
G5E972	Lamina-associated polypeptide 2, isoforms beta/gamma OS=Homo sapiens GN=TMPO PE=1 SV=1	46278	0	0	-	108	2	7	108

O95801	Tetratricopeptide repeat protein 4 OS=Homo sapiens GN=TTC4 PE=1 SV=3	44650	0	0	-	108	2	8	108
M0QYA2	PIH1 domain-containing protein 1 (Fragment) OS=Homo sapiens GN=PIH1D1 PE=1 SV=8	30652	115	2	9	222	5	9	107
A0A286YF22	D-3-phosphoglycerate dehydrogenase OS=Homo sapiens GN=PHGDH PE=1 SV=1	55903	0	0	-	105	2	7	105
H0YB37	Tetratricopeptide repeat protein 1 (Fragment) OS=Homo sapiens GN=TTC1 PE=1 SV=1	18890	0	0	-	100	3	8	100
D6RGK3	Transcription initiation factor TFIID subunit 9 (Fragment) OS=Homo sapiens GN=TAF9 PE=1 SV=8	15367	35	1	11	134	4	10	99
Q08752	Peptidyl-prolyl cis-trans isomerase D OS=Homo sapiens GN=PPID PE=1 SV=3	40738	0	0	-	98	2	8	98
H3BRU6	Poly(rC)-binding protein 2 (Fragment) OS=Homo sapiens GN=PCBP2 PE=1 SV=1	31691	79	2	9	174	5	9	95
Q9BX40	Protein LSM14 homolog B OS=Homo sapiens GN=LSM14B PE=1 SV=1	42045	0	0	-	94	2	7	94
H0YHC3	Nucleosome assembly protein 1-like 1 (Fragment) OS=Homo sapiens GN=NAP1L1 PE=1 SV=1	23403	0	0	-	92	2	7	92
Q96I24	Far upstream element-binding protein 3 OS=Homo sapiens GN=FUBP3 PE=1 SV=2	61602	0	0	-	90	2	6	90
A0A087WX29	TAR DNA-binding protein 43 (Fragment) OS=Homo sapiens GN=TARDBP PE=1 SV=1	26726	42	1	8	132	2	8	90
F8WE65	Peptidyl-prolyl cis-trans isomerase OS=Homo sapiens GN=PPIA PE=1 SV=1	13013	0	0	-	88	3	13	88
B4DM58	Dihydrofolate reductase OS=Homo sapiens GN=DHFR PE=1 SV=1	14491	0	0	-	88	2	12	88
P06748	Nucleophosmin OS=Homo sapiens GN=NPM1 PE=1 SV=2	32555	389	15	9	477	14	9	88
D6RBL5	Annexin OS=Homo sapiens GN=ANXA5 PE=1 SV=1	29319	0	0	-	85	2	10	85
G5E9Q4	Interferon-inducible double-stranded RNA-dependent protein kinase activator A OS=Homo sapiens GN=PRKRA PE=1 SV=1	11502	0	0	-	85	2	10	85
H0YCI4	Nucleosome assembly protein 1-like 4 (Fragment) OS=Homo sapiens GN=NAP1L4 PE=1 SV=1	23393	0	0	-	85	2	7	85
F2Z393	Transaldolase OS=Homo sapiens GN=TALDO1 PE=1 SV=1	35306	0	0	-	84	1	9	84

H0YKS4	Annexin (Fragment) OS=Homo sapiens GN=ANXA2 PE=1 SV=1	19518	0	0	-	83	2	4	83
P62191	26S proteasome regulatory subunit 4 OS=Homo sapiens GN=PSMC1 PE=1 SV=1	49154	0	0	-	81	2	7	81
A0A087WV01	Elongation factor 1-alpha OS=Homo sapiens GN=EEF1A1 PE=1 SV=1	46331	0	0	-	80	2	8	80
H3BS86	E3 ubiquitin-protein ligase CHIP (Fragment) OS=Homo sapiens GN=STUB1 PE=1 SV=8	24413	0	0	-	79	2	9	79
O95816	BAG family molecular chaperone regulator 2 OS=Homo sapiens GN=BAG2 PE=1 SV=1	23757	0	0	-	77	1	12	77
A0A0A0MSI0	Peroxiredoxin-1 (Fragment) OS=Homo sapiens GN=PRDX1 PE=1 SV=1	18964	0	0	-	76	2	12	76
P10599	Thioredoxin OS=Homo sapiens GN=TXN PE=1 SV=3	11730	0	0	-	73	1	4	73
D6RDG3	Transcription factor BTF3 (Fragment) OS=Homo sapiens GN=BTF3 PE=1 SV=3	11795	0	0	-	72	2	13	72
I3L397	Eukaryotic translation initiation factor 5A (Fragment) OS=Homo sapiens GN=EIF5A PE=1 SV=8	16009	227	7	13	299	10	13	72
A0A0C4DGB6	Serum albumin OS=Homo sapiens GN=ALB PE=1 SV=1	69181	45	1	8	116	3	7	71
Q9Y266	Nuclear migration protein nudC OS=Homo sapiens GN=NUDC PE=1 SV=1	38219	226	4	8	297	6	8	71
A0A0A0MTC4	Double-stranded RNA-binding protein Staufen homolog 2 OS=Homo sapiens GN=STAU2 PE=1 SV=1	43251	165	4	7	235	6	7	70
Q9Y3B4	Splicing factor 3B subunit 6 OS=Homo sapiens GN=SF3B6 PE=1 SV=1	14576	50	1	13	119	3	13	69
A0A0B4J2C3	Translationally-controlled tumor protein OS=Homo sapiens GN=TPT1 PE=1 SV=1	22559	0	0	-	67	2	12	67
Q08188	Protein-glutamine gamma-glutamyltransferase E OS=Homo sapiens GN=TGM3 PE=1 SV=4	76584	0	0	-	66	1	4	66
A0A087WWT3	Serum albumin OS=Homo sapiens GN=ALB PE=1 SV=1	45118	0	0	-	65	1	11	65
H0Y4Q3	Ran GTPase-activating protein 1 (Fragment) OS=Homo sapiens GN=RANGAP1 PE=1 SV=1	26891	0	0	-	64	2	6	64
O75663	TIP41-like protein OS=Homo sapiens GN=TIPRL PE=1 SV=2	31424	0	0	-	64	2	10	64
Q96GA3	Protein LTV1 homolog OS=Homo sapiens GN=LTV1 PE=1 SV=1	54821	0	0	-	61	1	6	61

Q5HY81	Ubiquitin-like protein 4A OS=Homo sapiens GN=UBL4A PE=1 SV=2	20538	34	1	13	95	2	13	61
F6WQW2	Ran-specific GTPase-activating protein OS=Homo sapiens GN=RANBP1 PE=1 SV=1	31884	83	2	10	143	3	10	60
B7ZAR1	T-complex protein 1 subunit epsilon OS=Homo sapiens GN=CCT5 PE=1 SV=1	55314	0	0	-	59	1	7	59
P31942	Heterogeneous nuclear ribonucleoprotein H3 OS=Homo sapiens GN=HNRNPH3 PE=1 SV=2	36903	0	0	-	57	1	9	57
H3BQB1	Adenine phosphoribosyltransferase (Fragment) OS=Homo sapiens GN=APRT PE=1 SV=1	17551	0	0	-	56	1	12	56
Q96G28	Cilia- and flagella-associated protein 36 OS=Homo sapiens GN=CFAP36 PE=1 SV=2	39422	0	0	-	53	1	8	53
M0QX69	NEDD8-conjugating enzyme Ubc12 (Fragment) OS=Homo sapiens GN=UBE2M PE=1 SV=8	8147	0	0	-	51	1	14	51
C9J0E4	Cystatin-A OS=Homo sapiens GN=CSTA PE=1 SV=1	7082	0	0	-	51	1	4	51

Table S1. DNA oligonucleotide sequences used for BioID2 constructs.

Construct	Sequence
EcoRI-Myc-BioID2-KpnI	GAATTCGCCACCATGGAACAAAAACTCATCTCAGAAGAGGATCTCGACTTCAAGAA CCTGATCTGGCTGAAGGAGGTGGACAGCACCCAGGAGAGACTGAAGGAGTGGAACG TGAGCTACGGCACCGCCCTGGTGGCCGACAGACAGACCAAGGGCAGAGGCGGCCTG GGCAGAAAGTGGCTGAGCCAGGAGGGCGGCCTGTACTTCAGCTTCCTGCTGAACCCC AAGGAGTTCGAGAACCTGCTGCAGCTGCCCCTGGTGCTGGGCCTGAGCGTGAGCGA GGCCCTGGAGGAGATCACCGAGATCCCCTTCAGCCTGAAGTGGCCCAACGACGTGTA CTTCCAGGAGAAGAAGGTGAGCGGCGTGCTGTGCGAGCTGAGCAAGGACAAGCTGA TCGTGGGCATCGGCATCAACGTGAACCAGAGAGAGATCCCCGAGGAGATCAAGGAC AGAGCCACCACCCTGTACGAGATCACCGGCAAGGACTGGGACAGAAAGGAGGTGCT GCTGAAGGTGCTGAAGAGAATCAGCGAGAACCTGAAGAAGTTCAAGGAGAAGAGCT TCAAGGAGTTCAAGGGCAAGATCGAGAGCAAGATGCTGTACCTGGGCGAGGAGGTG AAGCTGCTGGGCGAGGGCAAGATCACCGGCAAGCTGGTGGGCCTGAGCGAGAAGGG CGGCGCCCTGATCCTGACCGAGGAGGGCATCAAGGAGATCCTGAGCGGCGAGTTCA GCCTGAGAAGAAGCGGTACC
KpnI-(GGGS)3x-KpnI	AATTCGAGCTCATCGATGCATGGTACCGCCACCATGGAACAAAAACTCATCTCAGAA GAGGATCTCGCGGCCGCATCATTTCATGCGAGCCTCCT

Table S2. Primer sequences used for PCR and RT-qPCR.

Primer	Sequences
BioID2 F	CAAGAATTCGCCACCATGGAAC
BioID2 R	TTTGGTACCGCTTCTTCTCAGGCTG
BoDV L no ATG F	TCATTTCATGCGAGCCTCCTTCGCGAG
BoDV L no ATG XhoI R	GAGGGAAAAAGATCTGCTAGCTCGAGTCAATCAACCACCAAC
BioID2-KpnI-L1 F1	GCCTGAGAAGAAGCGGTACCTCATTTCATGCGAGCCTC
BioID2-KpnI-L1 R	ATTGAACATCTGATCCAACTGACGACAGAG
BioID2-KpnI-L2 F	GATCAGATGTTCAATTGCGGGTACTTCTTCAG
BioID2-KpnI-L2 R	AGTCTCCACGGGATGGGAGACGATGTGTGAG
BioID2-KpnI-L3-XhoI F	CATCCCGTGGAGACTCACGCCAAGGGCTCA
BioID2-KpnI-L3-XhoI R	GATCTGCTAGCTCGAGTCAATCAACCACCAAC
Myc-ALKBH8 F	CTGTCTCATCATTTTGGCAAAGAATTCATGGAACAAAAACTCATCTCAGAAGAGGATCTGGACAGCAACCATCAAAGT
Myc-ALKBH8 R	GAGGGAAAAAGATCTGCTAGCTCGAGTCAGGCCTTTTGAAGAATCAC
Myc-N6AMT1 F	CTGTCTCATCATTTTGGCAAAGAATTCATGAACAAAAACTCATCTCAGAAGAGGATCTGGCAGGGGAGAACTTCGCTA
Myc-N6AMT1 R	GAGGGAAAAAGATCTGCTAGCTCGAGCTAAGACTTGGTGAACTTGAG
Myc-TRMT11 F	CTGTCTCATCATTTTGGCAAAGAATTCATGGAACAAAAACTCATCTCAGAAGAGGATCTGGCGCTGTCGTGTACCCTT
Myc-TRMT11 R	GAGGGAAAAAGATCTGCTAGCTCGAGTCATTCCTGGGTGGATTTTTC
Myc-METTL5 F	CTGTCTCATCATTTTGGCAAAGAATTCATGGAACAAAAACTCATCTCAGAAGAGGATCTGAAGAAAGTAAGGCTTAAG
Myc-METTL5 R	GAGGGAAAAAGATCTGCTAGCTCGAGTTAAAAGGAAAACCGAATTAG
Myc-WBSCR22 F	CTGTCTCATCATTTTGGCAAAGAATTCATGGAACAAAAACTCATCTCAGAAGAGGATCTGGCGTCCCGCGGCCGGCGT
Myc-WBSCR22 R	GAGGGAAAAAGATCTGCTAGCTCGAGTTAGAAGCGGGGCTTGCGCT
Myc-TRMT112 F	CTGTCTCATCATTTTGGCAAAGAATTCATGGAACAAAAACTCATCTCAGAAGAGGATCTGAAACTGCTTACCCACAAT
Myc-TRMT112 R	GAGGGAAAAAGATCTGCTAGCTCGAGTCAACTCTCAGTTTCCTC
FLAG-RdRp F	CTGTCTCATCATTTTGGCAAAGAATTCATGGACTACAAGGACGACGATGACAAGTCATTTCATGCGAGCCTC
FLAG-RdRp R	GAGGGAAAAAGATCTGCTAGCTCGAGTCACGGAGGCAGCTCAACATACAAC
FLAG-Cap F	CTGTCTCATCATTTTGGCAAAGAATTCATGGACTACAAGGACGACGATGACAAGGCAATCATGCAGGACGAGTC
FLAG-Cap R	GAGGGAAAAAGATCTGCTAGCTCGAGTCACCACTCAGCACCCCTATATTG
FLAG-CTD F	CTGTCTCATCATTTTGGCAAAGAATTCATGGACTACAAGGACGACGATGACAAGCTGATATCAAAGCCAGTTAC
FLAG-CTD R	GAGGGAAAAAGATCTGCTAGCTCGAGTCAATCAACCACCAACAACTGCGTC

BoDV-1 gRNA-specific	TGTTGCGTTAACAACAAACCAATCAT
BoDV-1 agRNA-specific	TGCGCTACAACAAAGCAACAACC
GAPDH qPCR (new) F	GTATCGTGGAAGGACTCAT
GAPDH qPCR (new) R	AGTAGAGGCAGGGATGAT
BoDV-1 P qPCR F	ATGCATTGACCCAACCGGTA
BoDV-1 P qPCR R	ATCATTCGATAGCTGCTCCCTTC
BUD23 shRNA F	ACCGGGAGTGGAAGTTATCTGTCATTCAAGAGATGACAGATAACTTCCACTCTTTTTTGGGCCC
BUD23 shRNA R	CGAAGGGCCCAAAAAAGAGTGGAAGTTATCTGTCATCTCTTGAATGACAGATAACTTCCACTCC
Scramble shRNA F	ACCGGATTGCTCGAAGTGAATGGTTTCAAGAGAACCATTCACTTCGAGCAATTTTTTTGGGCCC
Scramble shRNA R	CGAAGGGCCCAAAAAAATTGCTCGAAGTGAATGGTTCTCTTGAAACCATTCACTTCGAGCAATC
EcoRI-BUD23 F	CTCATCATTTTGGCAAAGAATTCATGGCGTCCCGCGGCCGGCGT
EcoRI-BUD23wt R	ATAACTTCCACTCAGCCCAGTGCCACAGCCA
EcoRI-BUD23res R (new)	CATCACTTAAGTAACTTCCACTCAGCCCAG
BUD23wt-XhoI F	CTGGGCTGAGTGGAAGTTATCTGTCAGATG
BUD23res-XhoI F (new)	TGGAAGTTACTTAAGTGATGAAGGGCACTA
BUD23-XhoI R	AAAAAGATCTGCTAGCTCGAGTTAGAAGCGGGGCTTGCGCTTG
EcoRI-D117A R	GATGCAACCAGCAAATGTGCCTGGCTTGAA
D117A-XhoI F	GCACATTTGCTGGTTGCATCAGCATTTCTG
EcoRI-G63E R	CTCAGCCCAGTCTCACAGCCAATATCCAGC
G63E-XhoI F	GGCTGTGAGACTGGGCTGAGTGGAAGTTAT
GAPDH probe antisense F	ATATATTAATACGACTCACTATAGGGGGCAGTGATGGCATGGACTGTG
GAPDH probe antisense R	TGGTCACCAGGGCTGCTTTTAACTCTG
NARF probe 2 antisense F	ATATATTAATACGACTCACTATAGGGCAGCACCCGCTCGGCGTATC
NARF probe 2 antisense R	CTGATGACCAAGAGAATGTGTCAGCCGATG
gRNA probe antisense F	ATATATTAATACGACTCACTATAGGGTGTTGCGTTAACAACAAAC
gRNA probe antisense R	ATCACAACCCCAATTAGTAATGAGCAACAATG
gRNA probe antisense F2	ATATATTAATACGACTCACTATAGGGCGCTGGTCCAGGTGTGAT
gRNA probe antisense R2	ATCCAGCGGGAAGCCCAACCAGCAG

GAPDH whole F	ATGGGGAAGGTGAAGGTCGGAG
GAPDH whole R	TTACTCCTTGGAGGCCATGTGGGCCAT
NARF whole F	ATGAAGTGTGAGCACTGCACGCGCAAG
NARF whole R	TCACCACTTGATGTCCAGGCTGTGTG
BoDV-1 N0 F	CTAATTGGGGTTGTGATAGGATCGTCATC
BoDV-1 M2 R	GAGCTCCACATAGGAATGCTTTGAATTCATG
BoDV-1 M3 F	GAGACAATGAAGCTCATGATGGAGAAGGTG
BoDV-1 G4 R	GTTGAGACTTGCCTCAAACTCCTCTAG
BoDV-1 G5 F	GATTACAATGGACGGAAGTACTTTCTGAATG
BoDV L 2R	CTGCCTCATACCCTCTCCCATTGTC
BoDV L 3F	CACTGCCATGCTTTACCACGTTTATTATTCAG
BoDV L 4R	GAATGACTTGCCAATGAGAATCCCGAG
BoDV L 5F	CTCAATATAGGGGTGCTGAGTGGCTG
BoDV L 6R	CAATCAACCACCAACAACTGCGTCAATC

Table S3. Silencer Select siRNAs used for knockdown.

Gene	Assay ID
WBSCR22	s41529
TRMT112	s28230
HMGB1	s20254
Negative Control #1	4390844

Table S4. Antibodies used for protein-based experiments.

Name	Type	Catalogue number	Manufacturer
anti-BoDV-1 N	mouse monoclonal	HN132	
anti-BoDV-1 P	rabbit polyclonal	HB08	
anti-Myc	mouse monoclonal	M192-3	MBL
anti-FLAG	mouse monoclonal	F1804	Sigma-Aldrich
Mouse IgG Isotype Control		31903	Thermo Fisher Scientific
anti-TRMT112	mouse monoclonal	sc-398481	Santa Cruz Biotechnology
anti-WBSCR22	rabbit polyclonal	ab97911	Abcam
anti-ALKBH8	rabbit polyclonal	144-07142	RayBiotech
anti-N6AMT1	rabbit polyclonal	16211-1-AP	Proteintech
anti-METTL5	rabbit polyclonal	NBP1-56640	Novus Biologicals
anti-TRMT11	rabbit polyclonal	17555-1-AP	Proteintech
anti-Tubulin	mouse monoclonal	T5168	Sigma-Aldrich
anti-HMGB1	rabbit polyclonal	ab18256	Abcam
anti-mouse IgG HRP	goat polyclonal	115-035-003	Jackson ImmunoResearch
anti-rabbit IgG HRP	goat polyclonal	111-035-144	Jackson ImmunoResearch
anti-mouse IgG Alexa Fluor 555	goat polyclonal	A-21424	Thermo Fisher Scientific
anti-rabbi IgG Alexa Fluor 488	goat polyclonal	A-11034	Thermo Fisher Scientific

Table S5. DNA oligonucleotide sequences used for shRNA lentiviral vector constructs.

shRNA	Target sequence	Oligonucleotide sequence
BUD23	GAGTGGAAGTTATCTGTCA	F:ACCGGGAGTGGAAGTTATCTGTCATTCAAGAGATGACAGATA ACTTCCACTCTTTTTTGGGCCC
		R:CGAAGGGCCCAAAAAAGAGTGGAAGTTATCTGTCATCTCTTG AATGACAGATAACTTCCACTCC
Scramble	ATTGCTCGAAGTGAATGGT	F:ACCGGATTGCTCGAAGTGAATGGTTTCAAGAGAACCATTCACT TCGAGCAATTTTTTTGGGCCC
		R:CGAAGGGCCCAAAAAAATTGCTCGAAGTGAATGGTTCTCTTG AAACCATTCACTTCGAGCAATC

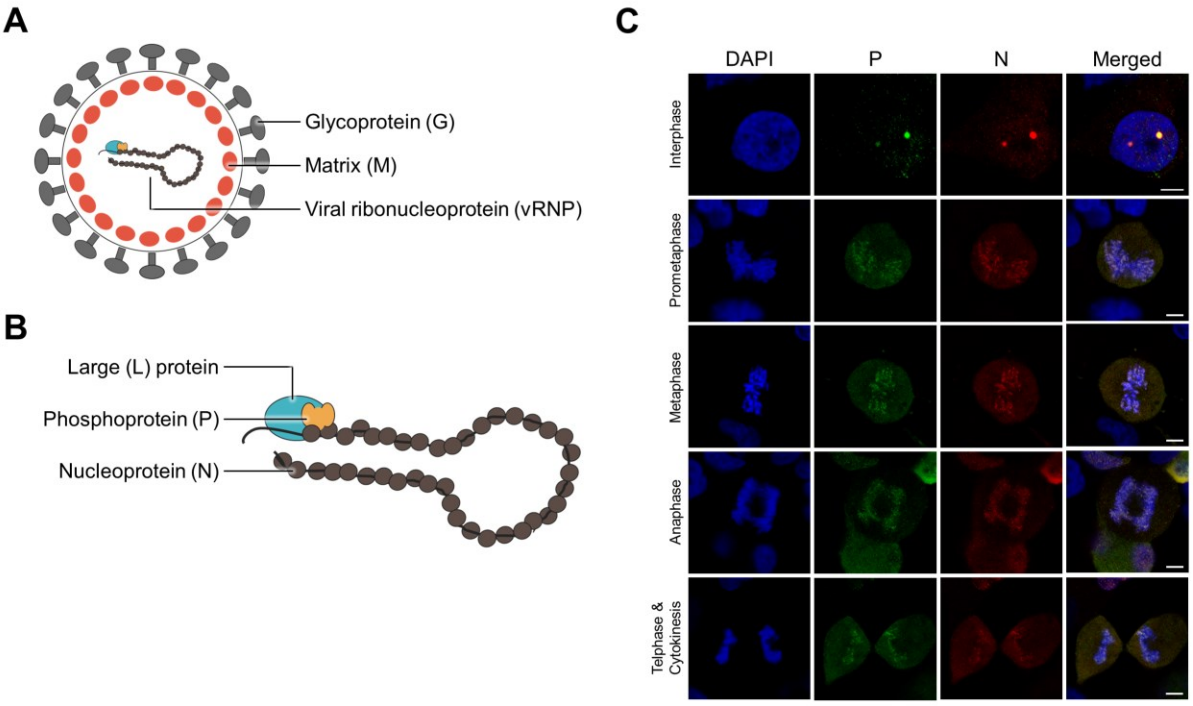
A
Glycoprotein (G)
Matrix (M)
Viral ribonucleoprotein (vRNP)
B
Large (L) protein
Phosphoprotein (P)
Nucleoprotein (N)
C
DAPI
P
N
Merged
Interphase
Prometaphase
Metaphase
Anaphase
Telphase &
Cytokinesis

Fig. 1

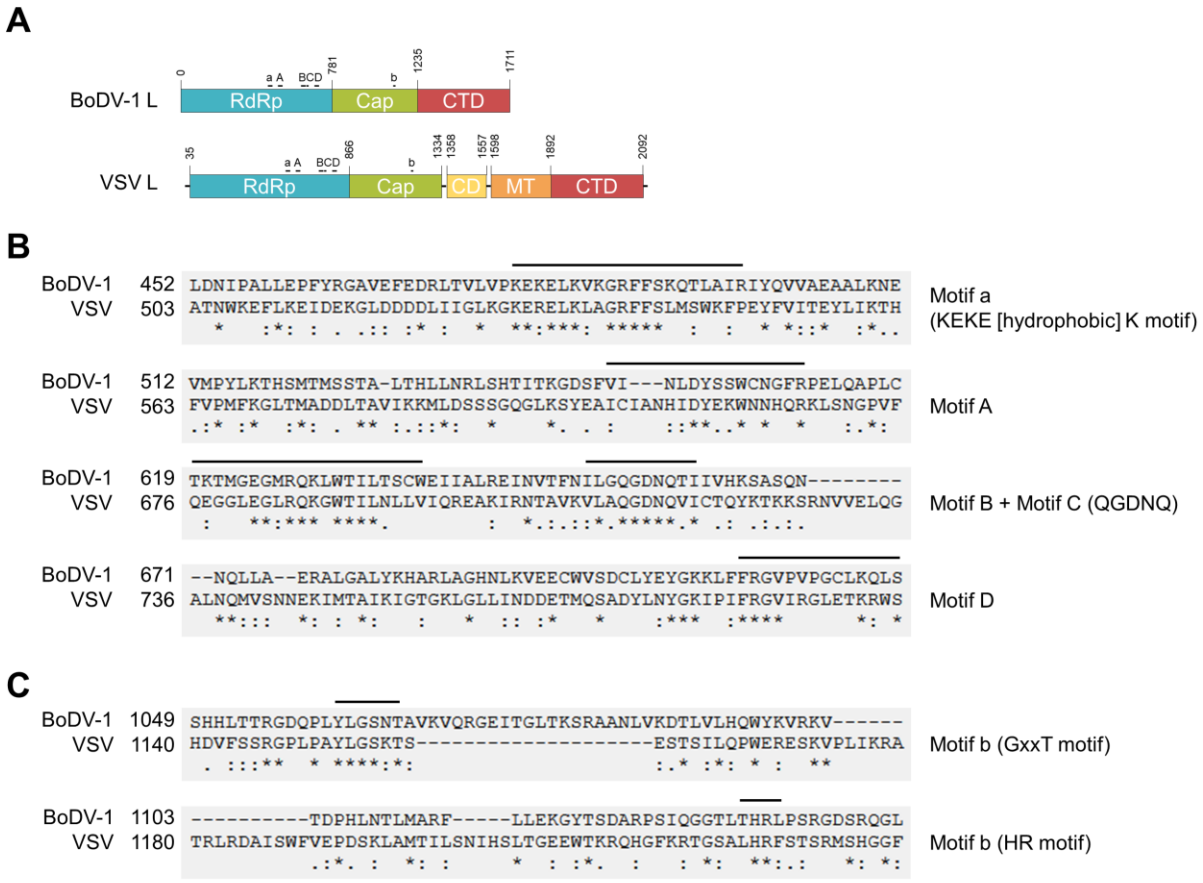
A
BoDV-1 L
0
a A
BCD
781
b
1235
1711
RdRp
Cap
CTD
VSV L
35
a A
BCD
866
b
1334
1358
1557
1598
1892
2092
RdRp
Cap
CD
MT
CTD
B
BoDV-1 452 LDNIPALLEPFYRGAVEFEDRLTVLVPKEKELKVKGRFFSKQTLAIRIYQVVAEAALKNE
VSV 503 ATNWKEFLKEIDEKGLDDDDLIIGLKGKERELKLAGRFFSLMSWKFPEYFVITEYLIKTH
Motif a
(KEKE [hydrophobic] K motif)
BoDV-1 512 VMPYLKTHSMTMSSTA-LTHLLNRLSHTITKGDSFVI---NLDYSSWCNGFRPELQAPLC
VSV 563 FVPMFKGLTMADDLTAVIKKMLDSSSGQGLKSYEAICIANHIDYEKWNNHQRKLSNGPVF
Motif A
BoDV-1 619 TKTMGEGMRQKLWTILTSCWEIIALREINVTFNILGQGDNQTIIVHKSASQN--------
VSV 676 QEGGLEGLRQKGWTILNLLVIQREAKIRNTAVKVLAQGDNQVICTQYKTKKSRNVVELQG
Motif B + Motif C (QGDNQ)
BoDV-1 671 --NQLLA--ERALGALYKHARLAGHNLKVEECWVSDCLYEYGKKLFFRGVPVPGCLKQLS
VSV 736 ALNQMVSNNEKIMTAIKIGTGKLGLLINDDETMQSADYLNYGKIPIFRGVIRGLETKRWS
Motif D
C
BoDV-1 1049 SHHLTTRGDQPLYLGSNTAVKVQRGEITGLTKSRAANLVKDTLVLHQWYKVRKV------
VSV 1140 HDVFSSRGPLPAYLGSKTS--------------------ESTSILQPWERESKVPLIKRA
Motif b (GxxT motif)
BoDV-1 1103 ----------TDPHLNTLMARF-----LLEKGYTSDARPSIQGGTLTHRLPSRGDSRQGL
VSV 1180 TRLRDAISWFVEPDSKLAMTILSNIHSLTGEEWTKRQHGFKRTGSALHRFSTSRMSHGGF
Motif b (HR motif)

Fig. 2

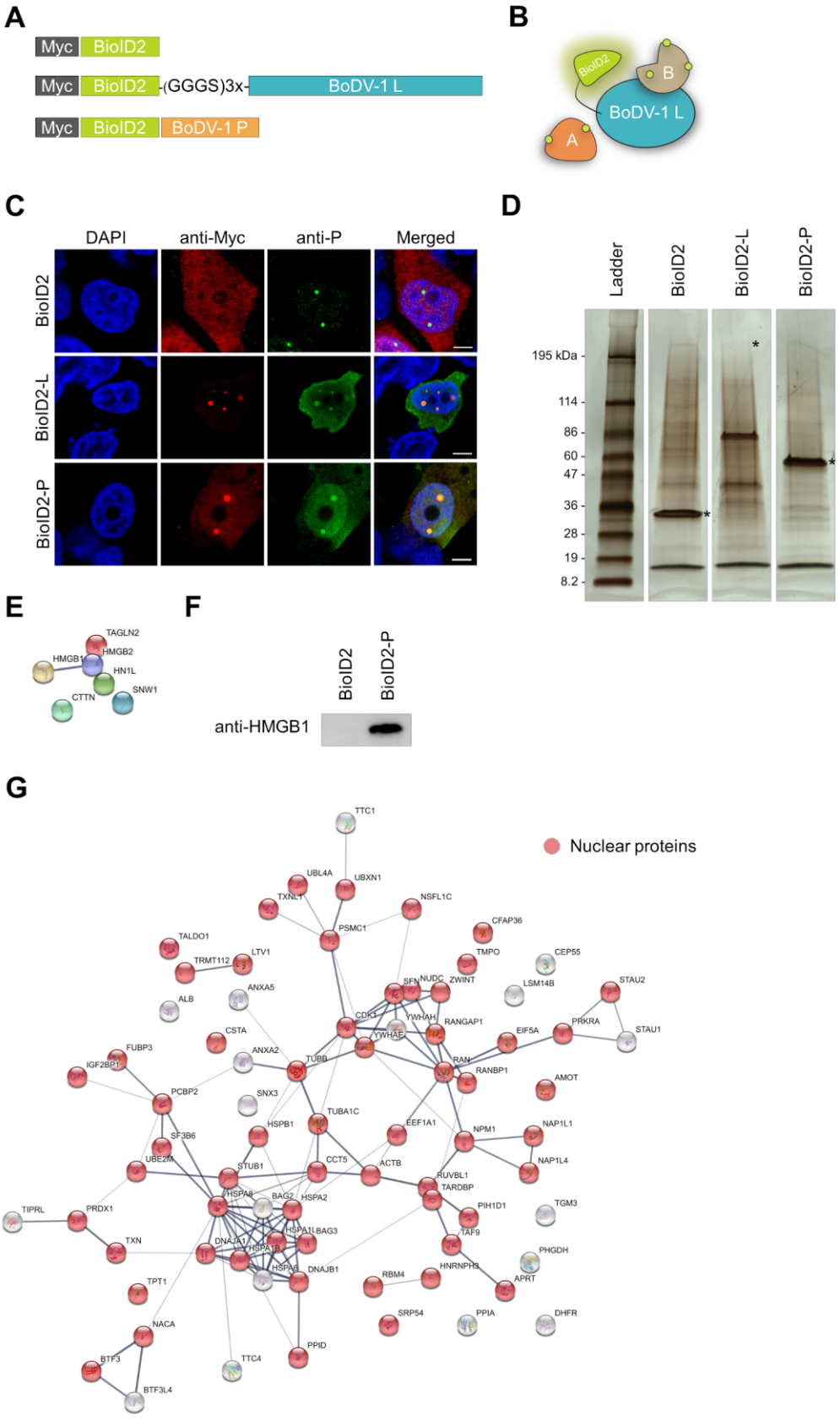
A
Myc
BioID2
Myc
BioID2
-(GGGS)3x-
BoDV-1 L
Myc
BioID2
BoDV-1 P
B
BioID2
B
BoDV-1 L
A
C
DAPI
anti-Myc
anti-P
Merged
BioID2
BioID2-L
BioID2-P
D
Ladder
BioID2
BioID2-L
BioID2-P
195 kDa
114
86
60
47
36
28
19
8.2
E
TAGLN2
HMGB1
HMGB2
HN1L
SNW1
CTTN
F
BioID2
BioID2-P
anti-HMGB1
G
Nuclear proteins
TTC1
UBL4A
UBXN1
TXNL1
NSFL1C
PSMC1
CFAP36
TALDO1
TRMT112
LTV1
TMPO
CEP55
SFN
NUDC
ZWINT
LSM14B
STAU2
ANXA5
ALB
CDK1
YWHAH
YWHAE
RANGAP1
EIF5A
PRKRA
STAU1
CSTA
ANXA2
TUBB
RAN
RANBP1
FUBP3
IGF2BP1
AMOT
PCBP2
SNX3
TUBA1C
HSPB1
EEF1A1
NPM1
NAP1L1
SF3B6
UBE2M
STUB1
CCT5
ACTB
NAP1L4
RUVBL1
TARDBP
HSPA8
BAG2
HSPA2
PIH1D1
TGM3
TIPRL
PRDX1
TAF9
TXN
DNAJA1
HSPA1A
HSPA1L
BAG3
PHGDH
HSPA5
DNAJB1
HNRNPH3
RBM4
APRT
TPT1
SRP54
PPIA
DHFR
NACA
PPID
BTF3
TTC4
BTF3L4

Fig. 3

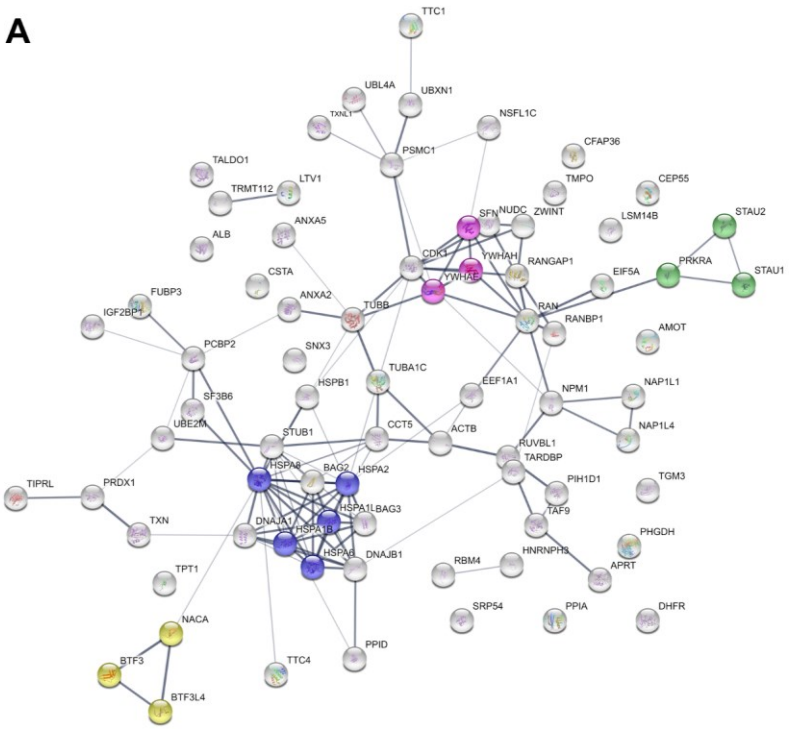

Pfam domain	Description	FDR
PF00012	Hsp70 protein	8.95e-07
PF16482	Staufen C-terminal domain	3.79e-05
PF01849	NAC domain	7.91e-05
PF00244	14-3-3 protein	1.30e-04

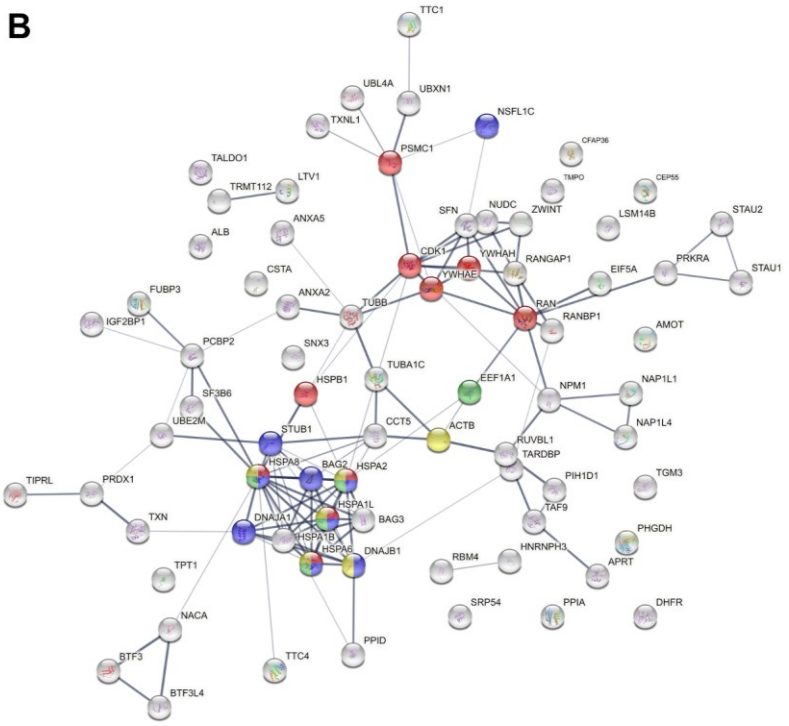

KEGG pathway	Description	FDR
hsa05169	Epstein-Barr virus infection	5.19e-07
hsa04141	Protein-processing in endoplasmic reticulum	7.94e-07
hsa05134	Legionellosis	8.49e-05
hsa05164	Influenza A	1.20e-03

Fig. 4

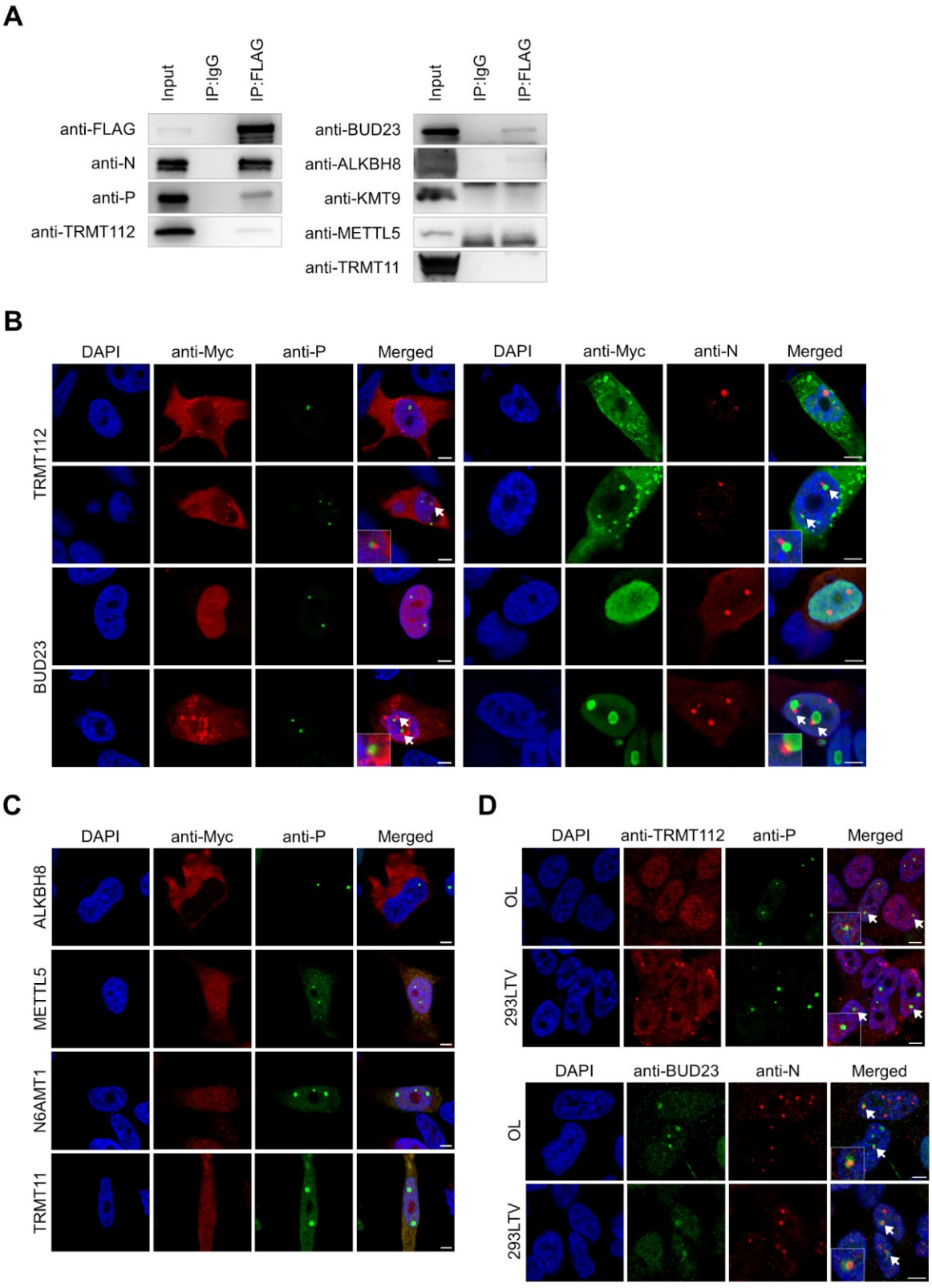
A
Input
IP:IgG
IP:FLAG
anti-FLAG
anti-N
anti-P
anti-TRMT112
anti-BUD23
anti-ALKBH8
anti-KMT9
anti-METTL5
anti-TRMT11
B
DAPI
anti-Myc
anti-P
Merged
anti-N
TRMT112
BUD23
C
ALKBH8
METTL5
N6AMT1
TRMT11
D
anti-TRMT112
OL
293LTV
anti-BUD23

Fig. 5

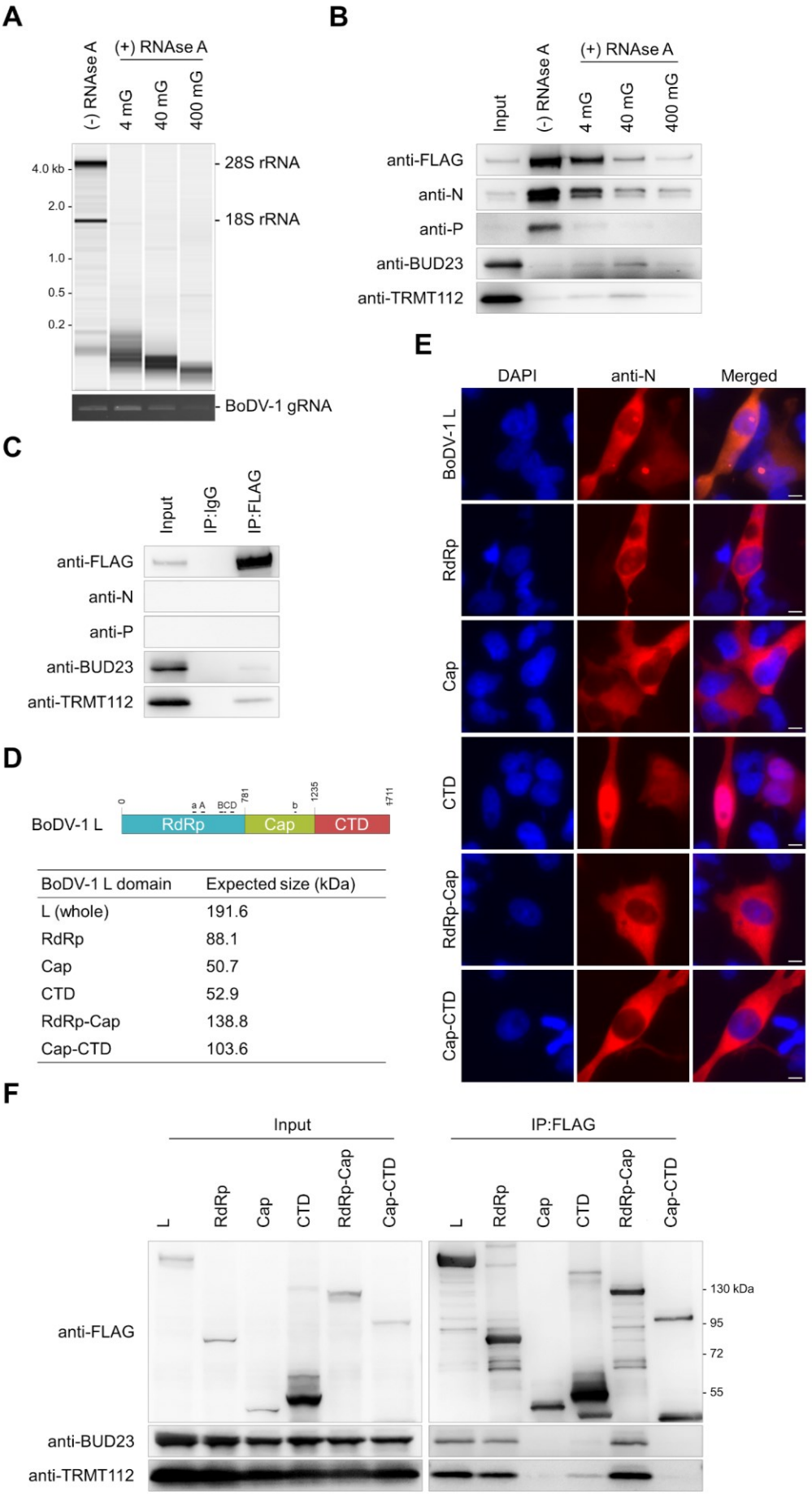

BoDV-1 L domain	Expected size (kDa)
L (whole)	191.6
RdRp	88.1
Cap	50.7
CTD	52.9
RdRp-Cap	138.8
Cap-CTD	103.6

Fig. 6

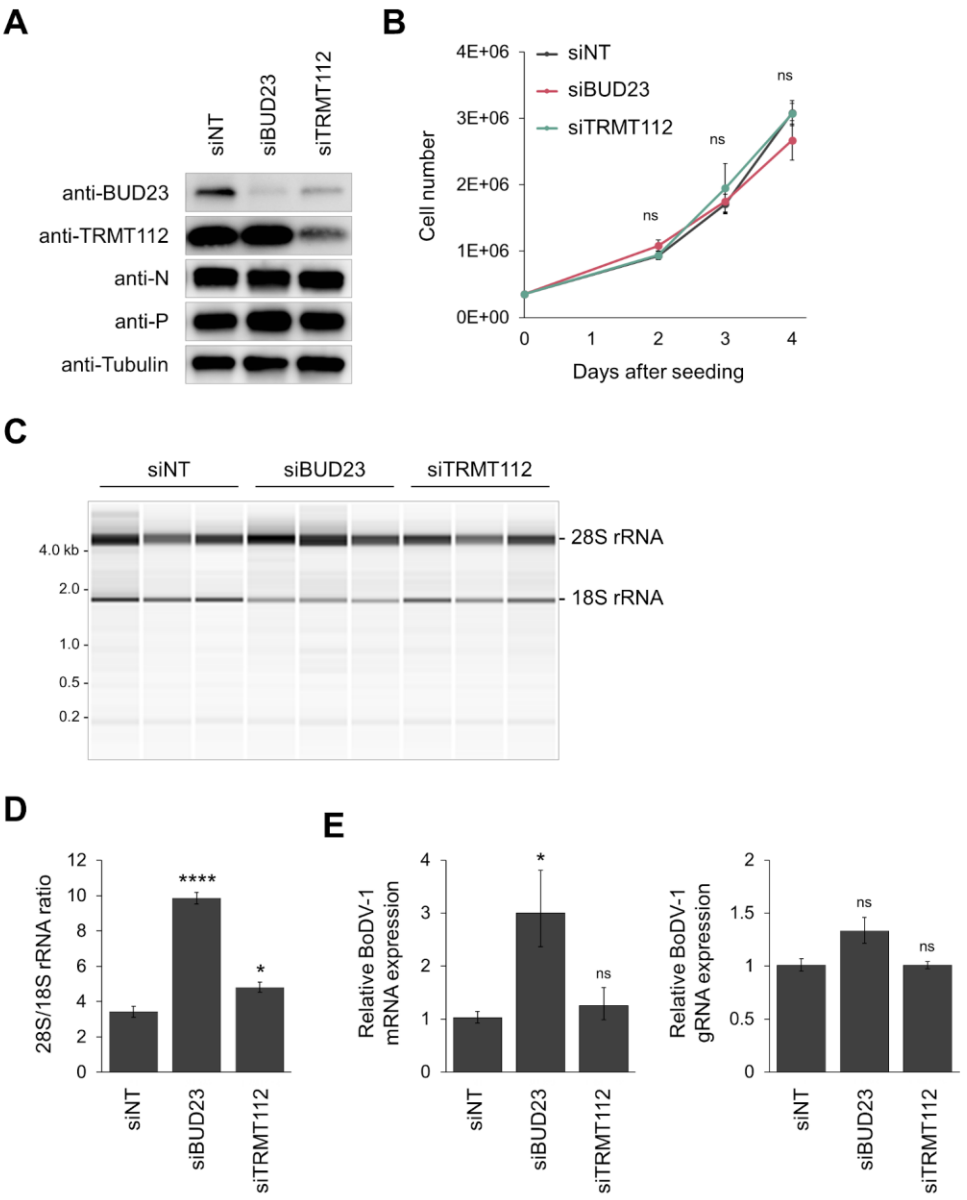
A
siNT
siBUD23
siTRMT112
anti-BUD23
anti-TRMT112
anti-N
anti-P
anti-Tubulin
B
siNT
siBUD23
siTRMT112
Cell number
4E+06
3E+06
2E+06
1E+06
0E+00
0
1
2
3
4
Days after seeding
ns
ns
ns
C
siNT
siBUD23
siTRMT112
4.0 kb
2.0
1.0
0.5
0.2
28S rRNA
18S rRNA
D
28S/18S rRNA ratio
****
*
E
Relative BoDV-1 mRNA expression
*
ns
Relative BoDV-1 gRNA expression
ns
ns
siNT
siBUD23
siTRMT112

Fig. 7

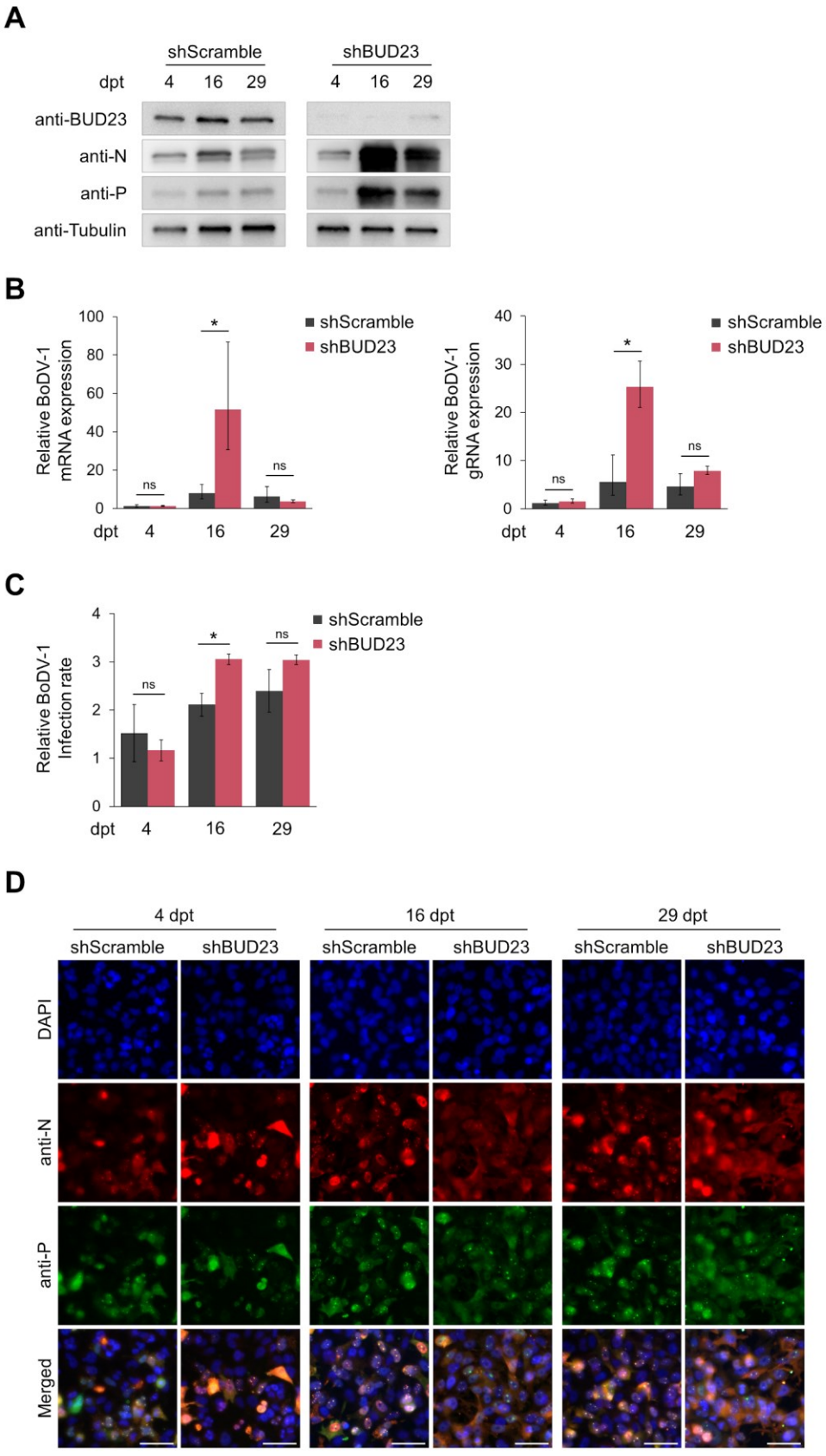
A
shScramble
shBUD23
dpt
4
16
29
4
16
29
anti-BUD23
anti-N
anti-P
anti-Tubulin
B
Relative BoDV-1 mRNA expression
100
80
60
40
20
0
*
ns
ns
shScramble
shBUD23
dpt
4
16
29
Relative BoDV-1 gRNA expression
40
30
20
10
0
*
ns
ns
shScramble
shBUD23
dpt
4
16
29
C
Relative BoDV-1 Infection rate
4
3
2
1
0
ns
*
ns
shScramble
shBUD23
dpt
4
16
29
D
4 dpt
16 dpt
29 dpt
shScramble
shBUD23
shScramble
shBUD23
shScramble
shBUD23
DAPI
anti-N
anti-P
Merged

Fig. 8

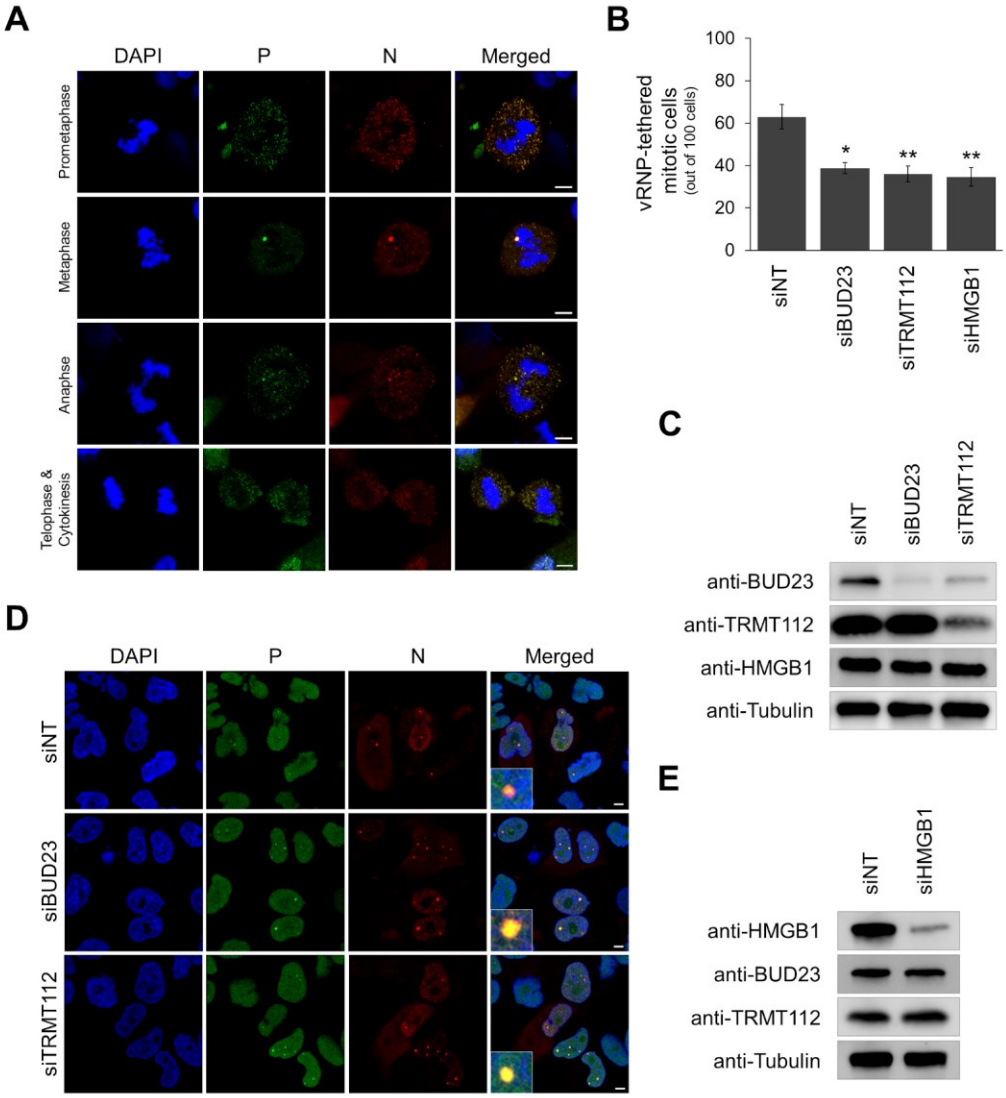
A
DAPI
P
N
Merged
Prometaphase
Metaphase
Anaphse
Telophase & Cytokinesis
B
vRNP-tethered mitotic cells (out of 100 cells)
100
80
60
40
20
0
*
**
**
siNT
siBUD23
siTRMT112
siHMGB1
C
siNT
siBUD23
siTRMT112
anti-BUD23
anti-TRMT112
anti-HMGB1
anti-Tubulin
D
DAPI
P
N
Merged
siNT
siBUD23
siTRMT112
E
siNT
siHMGB1
anti-HMGB1
anti-BUD23
anti-TRMT112
anti-Tubulin

Fig. 9

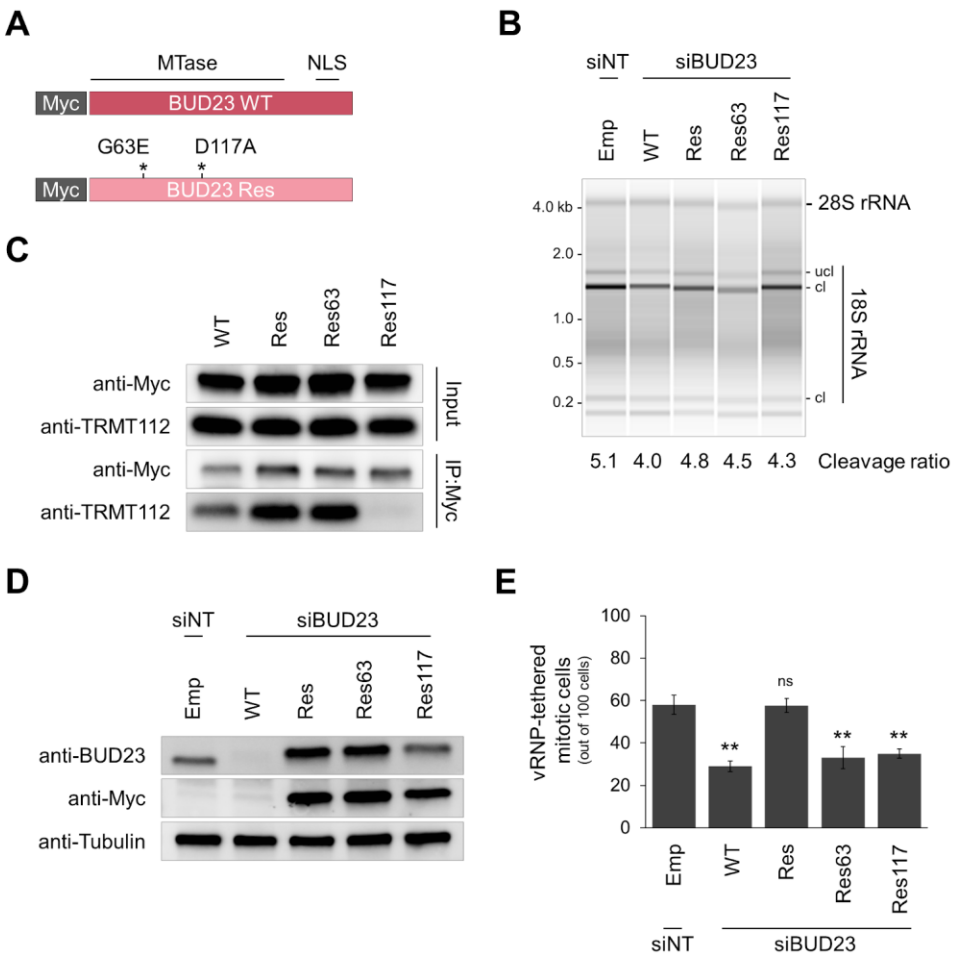
A
MTase
NLS
Myc
BUD23 WT
G63E
D117A
Myc
BUD23 Res
B
siNT
siBUD23
Emp
WT
Res
Res63
Res117
4.0 kb
2.0
1.0
0.5
0.2
28S rRNA
ucl
cl
18S rRNA
cl
5.1
4.0
4.8
4.5
4.3
Cleavage ratio
C
WT
Res
Res63
Res117
anti-Myc
anti-TRMT112
Input
anti-Myc
anti-TRMT112
IP:Myc
D
siNT
siBUD23
Emp
WT
Res
Res63
Res117
anti-BUD23
anti-Myc
anti-Tubulin
E
vRNP-tethered mitotic cells
(out of 100 cells)
100
80
60
40
20
0
ns
**
**
**
Emp
WT
Res
Res63
Res117
siNT
siBUD23

Fig. 10

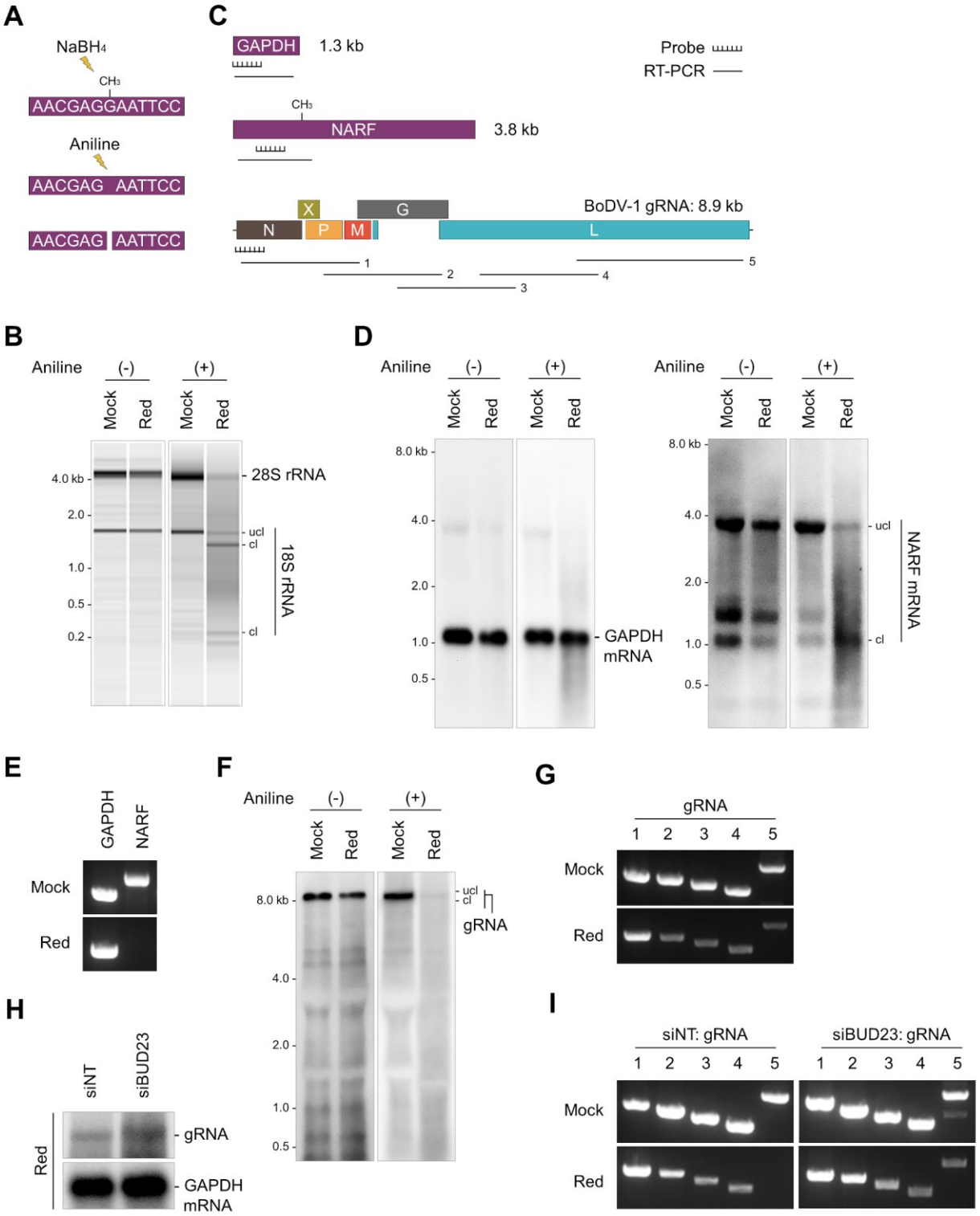
A
NaBH4
CH3
AACGAGGAATTCC
Aniline
AACGAG AATTCC
AACGAG AATTCC
C
GAPDH
1.3 kb
Probe
RT-PCR
CH3
NARF
3.8 kb
X
G
BoDV-1 gRNA: 8.9 kb
N
P
M
L
1
2
3
4
5
B
Aniline
(-)
(+)
Mock
Red
Mock
Red
4.0 kb
2.0
1.0
0.5
0.2
28S rRNA
ucl
cl
cl
18S rRNA
D
Aniline
(-)
(+)
Mock
Red
Mock
Red
8.0 kb
4.0
2.0
1.0
0.5
GAPDH
mRNA
Aniline
(-)
(+)
Mock
Red
Mock
Red
8.0 kb
4.0
2.0
1.0
0.5
ucl
cl
NARF mRNA
E
GAPDH
NARF
Mock
Red
F
Aniline
(-)
(+)
Mock
Red
Mock
Red
8.0 kb
4.0
2.0
1.0
0.5
ucl
cl
gRNA
G
gRNA
1 2 3 4 5
Mock
Red
H
siNT
siBUD23
Red
gRNA
GAPDH
mRNA
I
siNT: gRNA
siBUD23: gRNA
1 2 3 4 5
1 2 3 4 5
Mock
Red

Fig. 11

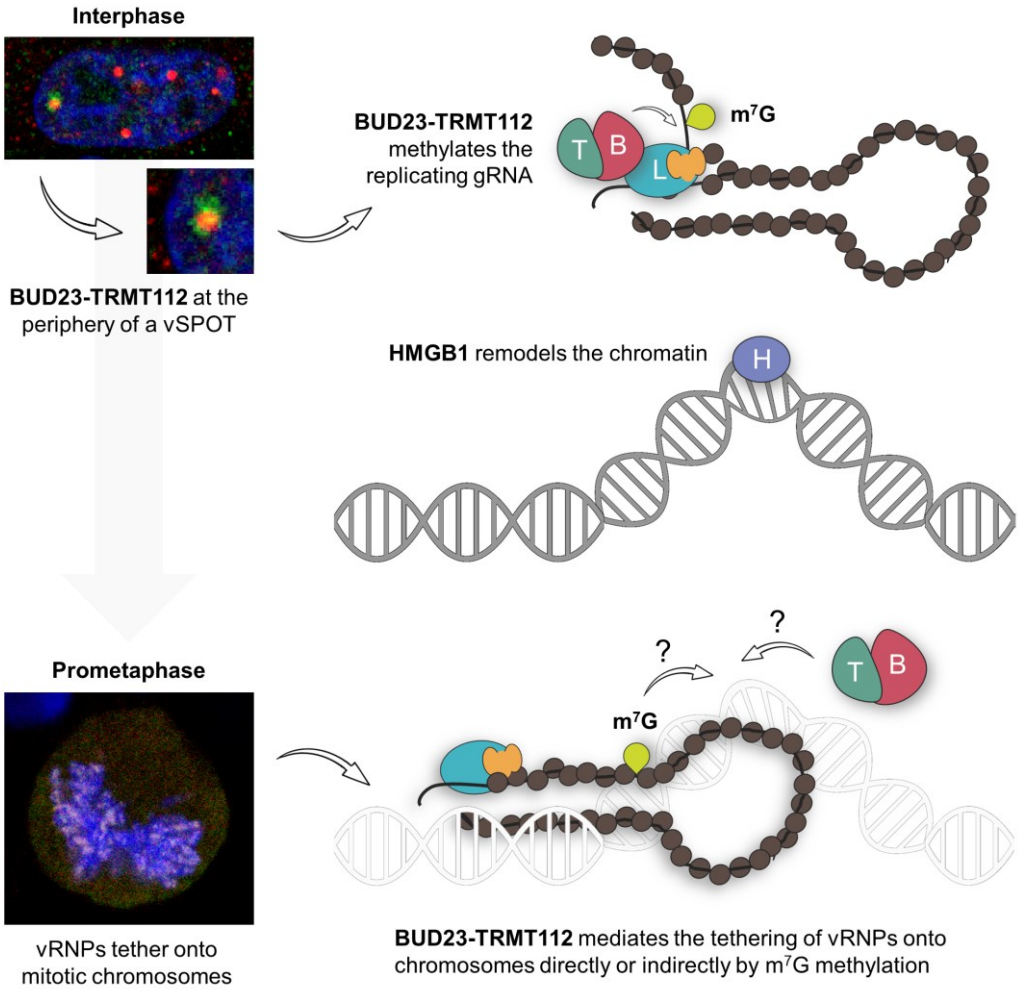
Interphase
BUD23-TRMT112 at the periphery of a vSPOT
BUD23-TRMT112 methylates the replicating gRNA
m7G
T
B
L
HMGB1 remodels the chromatin
H
Prometaphase
vRNPs tether onto mitotic chromosomes
?
?
T
B
m7G
BUD23-TRMT112 mediates the tethering of vRNPs onto chromosomes directly or indirectly by m7G methylation

Fig. 12

Figure Legends

Figure 1. Nuclear infection of BoDV-1.

(A) Schematic diagram of BoDV-1 virion with G and M proteins surrounding the vRNP. (B) Schematic diagram of BoDV-1 vRNP consisting of L, P, and the N protein-encapsidated gRNA. (C) Representative images of vSPOTs at interphase and tethered vRNPs at different phases of mitosis, in BoDV-1-infected OL cells. vRNPs were stained using anti-N and anti-P antibodies, and chromosomes were stained using DAPI. Scale bars: 5 μm.

Figure 2. Alignment of conserved motifs between BoDV-1 L and VSV L.

(A) Schematic diagram of the domain organizations and conserved motifs in BoDV-1 L and VSV L after MAFFT alignment. RdRp: RNA-dependent RNA polymerase domain, Cap: PRNTase or Capping domain, CD: Connector domain, MT: Methyltransferase domain, CTD: C-terminal domain. Conserved motifs in the (B) RdRp and (C) Cap domain of BoDV-1 L and VSV L.

Figure 3. Identification of host protein interactors of BoDV-1 L by proximity-dependent biotinylation.

(A) Schematic diagram of BioID2, BioID2-L, and BioID2-P constructs. Myc-tagged BioID2 is fused to N-terminal region of BoDV-1 P, or in case of BoDV-1 L, with (GGGS)3x flexible linker, to construct BioID2-P and BioID2-L, respectively. (B) Schematic diagram of the biotinylation of host proteins interacting transiently or bound to BoDV-1 L by BioID2. (C) Localization of BioID2, BioID2-P, and BioID2-L in BoDV-1-infected OL cells. BioID2 recombinant proteins were stained using anti-Myc antibody, vSPOTs were stained using anti-P antibody, and nuclei were counterstained using DAPI. (D) Silver staining of biotinylated proteins. Asterisks represent biotinylated BioID2, BioID2-L, and BioID2-P. (E) STRING

network showing the host protein interactors of BoDV-1 P. See also Table 1. (F) Biotinylated HMGB1 by BioID2-P after immunoprecipitation by streptavidin beads, as shown by Western blotting. BioID2 served as negative control. (G) STRING network showing the host protein interactors of BoDV-1 L. Red color indicates nuclear proteins. See also Table 2. (E,G) Line thickness indicates strength of data support for the interaction.

Figure 4. Functional enrichments within the network of host protein interactors of BoDV-1 L.

(A) Top enriched Pfam domains and (B) KEGG pathways within the network of host protein interactors of BoDV-1 L. Color assignment indicates assigned enrichment to which the protein belongs. False-discovery rate (FDR) indicates strength of support for the enrichment.

Figure 5. Interaction of TRMT112 and MTase partner BUD23 with BoDV-1 vRNPs.

(A) Co-immunoprecipitation of endogenous TRMT112 and its RNA MTase partners ALKBH8, BUD23, KMT9, METTL5, and TRMT11 with FLAG-BoDV-1 L from lysate of BoDV-1-infected 293LTV cells, as shown by Western blotting. BoDV-1 N and P served as positive controls. (B) Localization of Myc-BUD23 and Myc-TRMT112 in BoDV-1-infected OL cells. (C) Localization of other Myc-tagged RNA MTAses in BoDV-1-infected OL cells. (B,C) Myc-tagged proteins were stained using anti-Myc antibody, vSPOTs were stained using anti-P or anti-N antibody, and nuclei were counterstained using DAPI. (D) Localization of endogenous TRMT112 and BUD23 in BoDV-1-infected OL and 293LTV cells. TRMT112 were stained using anti-TRMT112 antibody, BUD23 were stained using anti-BUD23 antibody, vSPOTs were stained using anti-P or anti-N antibody, and nuclei were counterstained using DAPI. (B,D) White arrows indicate peripheral interaction. Scale bars: 5 μm.

Figure 6. Binding of BUD23-TRMT112 to RdRp domain of BoDV-1 L.

(A) Total RNA and BoDV-1 gRNA degradation after addition of increasing concentration of RNase A in the lysate of BoDV-1-infected 293LTV cells, as shown by RNA electrophoresis and RT-PCR, respectively. (B) BUD23 and TRMT112, and viral proteins BoDV-1 N and BoDV-1 P, were co-immunoprecipitated with FLAG-BoDV-1 L after RNase treatment, as shown by Western blotting. (C) Co-immunoprecipitation of BUD23 and TRMT112 with FLAG-BoDV-1 L from lysate of non-infected 293LTV cells. BoDV-1 N and P served as negative controls. (D) Upper panel shows the schematic diagram of the domain organization and conserved motifs of BoDV-1 L. RdRp: RNA-dependent RNA polymerase domain, Cap: Capping domain, CTD: C-terminal domain. Lower panel shows the constructed FLAG-BoDV-1 L domain truncations and expected sizes. (E) Localization of FLAG-BoDV-1 L domain truncations in non-infected OL cells. FLAG-tagged proteins were stained using anti-FLAG antibody and nuclei were counterstained using DAPI. Scale bars: 5 μm. (F) Co-immunoprecipitation of BUD23 and TRMT112 with FLAG-BoDV-1 L domain truncations from lysate of non-infected 293LTV cells, as shown by Western blotting.

Figure 7. Transient knockdown of BUD23-TRMT112 and effect on BoDV-1 replication.

(A) BoDV-1 and P expression levels as shown by Western blotting, after BUD23 or TRMT112 siRNA-induced knockdown in BoDV-1-infected OL cells. Tubulin served as loading control. (B) Proliferation of BoDV-1-infected OL cells after knockdown. (C) 28S and 18S rRNA levels after knockdown, as shown by RNA electrophoresis. (D) 28S/18S rRNA ratio quantified from (C). (E) Quantification of BoDV-1 mRNA and gRNA expression levels after knockdown, by RT-qPCR. (B,D,E) Average of three independent biological replicates ± SEM is shown. One-way ANOVA followed by Dunnett's multiple comparison test were used for the statistical

analysis. ****p<0.0001, *p<0.05, ns: not significant. (A-D) Non-targeting (NT) siRNA was used as negative control.

Figure 8. Prolonged knockdown of BUD23 and effect on BoDV-1 replication.

(A) BoDV-1 N and P expression levels as shown by Western blotting, after BUD23 shRNA-induced knockdown in BoDV-1-infected OL cells, at different days post-transduction (dpt). Tubulin served as loading control. (B) Quantification of BoDV-1 mRNA and gRNA expression levels after knockdown, by RT-qPCR. (C) Quantification of BoDV-1 infection after knockdown, by IFA in (D). vSPOTs were stained using anti-N and anti-P antibodies, and nuclei were counterstained using DAPI. Scale bars: 50 μm. (B,C) Average of three independent biological replicates ± SEM is shown. One-way ANOVA followed by Šidák's multiple comparisons test were used for the statistical analysis. *p<0.05, ns: not significant. (A-D) Scramble shRNA was used as negative control.

Figure 9. Role of BUD23-TRMT112 in the chromosomal tethering of BoDV-1 vRNPs.

(A) Representative images of untethered vRNPs at different phases of mitosis, in BoDV-1-infected OL cells. vRNPs were stained using anti-N and anti-P antibodies, and chromosomes were stained using DAPI. (B) Number of vRNP-tethered mitotic cells out of 100 cells after BUD23 or TRMT112 siRNA-induced knockdown. vRNPs were stained using anti-N antibodies and chromosomes were counterstained using DAPI. HMGB1 siRNA was used as positive control. Average of three independent biological replicates ± SEM is shown. One-way ANOVA followed by Dunnett's multiple comparison test were used for the statistical analysis. **p<0.01, *p<0.05. (C) HMGB1 expression level as shown by Western blotting, after siRNA-induced knockdown in BoDV-1-infected OL cells. (D) Localization of HMGB1 after siRNA-induced knockdown in BoDV-1-infected OL cells. HMGB1 were stained using anti-

HMGB1 antibody, vSPOTs were stained using anti-N antibodies, and nuclei were counterstained using DAPI. (A,D) Scale bars: 5 μm. (E) BUD23 and TRMT112 expression levels as shown by Western blotting, after HMGB1 siRNA-induced knockdown. (C,E) Tubulin served as loading control. (B-E) Non-targeting (NT) siRNA was used as negative control.

Figure 10. MTase activity of BUD23 is indispensable in the chromosomal tethering process.

(A) Schematic diagram of the BUD23 constructs. Upper image represents the BUD23 with wild type (WT) sequence while lower image represents the BUD23 with silent mutations to render it resistant (Res) to BUD23 siRNA-induced knockdown. MTase-defective Res63 (G63E) and TRMT112-binding impaired Res117 (D117A) were then constructed. All constructs contain an N-terminal Myc tag. MTase: Methyltransferase domain. NLS: Nuclear localization signal. (B) m^7G1639 methylation level in 18S rRNA following the expression of BUD23 Res variants, determined by $NaBH_4$/aniline treatment and RNA electrophoresis. (C) Co-immunoprecipitation of TRMT112 with BUD23 Res variants, as shown by Western blotting. (D) Expression level of BUD23 Res variants prior to (E), as shown by Western blotting. (E) Number of vRNP-tethered mitotic cells out of 100 cells, following the expression of BUD23 Res variants in BoDV-1-infected OL cells. vRNPs were stained using anti-N antibody and chromosomes were counterstained using DAPI. One-way ANOVA followed by Dunnett's multiple comparison test were used for the statistical analysis. $^{**}p<0.01$, ns: not significant. (B,D,E) siRNA-induced knockdown preceded expression of empty vector (Emp) or BUD23 variants.

Figure 11. Internal m^7G methylation of BUD23 in BoDV-1 gRNA.

(A) Schematic diagram of m^7G site-specific cleavage of RNA by $NaBH_4$ and aniline treatment. (B) Cleavage of 18S rRNA as shown by RNA electrophoresis. 28S rRNA and 18S rRNA (uncleaved or ucl) are represented by 5.0 and 1.9 kb bands, respectively. Cleaved (cl) 18S rRNA are represented by 1.6 kb and 0.23 kb bands. (C) Schematic diagram of the target sites of DIG-labeled RNA probes for Northern blotting, and RT-PCR, of GAPDH mRNA, NARF mRNA, and BoDV-1 gRNA. Canonical NARF mRNA transcript contains m^7G1073. (D) Cleavage of GAPDH mRNA and NARF mRNA, as shown by Northern blotting. Canonical mRNA transcripts of GAPDH and NARF are represented by 1.3 kb and 3.8 kb bands, respectively. Cleaved NARF mRNA is represented by 1.0 kb band. (E) Cleavage of GAPDH mRNA and NARF mRNA, as shown by RT-PCR. (F) Cleavage of BoDV-1 gRNA, as shown by Northern blotting. Uncleaved gRNA is represented by 8.9 kb band, while cleaved gRNA is represented by a slightly lower 8.9 kb band. (G) Cleavage of BoDV-1 gRNA, as shown by RT-PCR of segments. Cleavage of BoDV-1 gRNA after BUD23-siRNA induced knockdown, as shown by (H) Northern blotting and (I) RT-PCR. (B,D-I) Total RNA were treated with $NaBH_4$ under mock or reduced (red) conditions, and then treated in the absence or presence of aniline.

Figure 12. Summary.

During the interphase stage, BoDV-1 form vSPOTs in the cell nucleus, where viral transcription and viral replication take place. BUD23-TRMT112 then interact along the periphery of the vSPOTs, and specifically bind to the RdRp domain of BoDV-1 L where it might methylate the internal m^7G in BoDV-1 gRNA, possibly during replication. During the prometaphase stage, the vSPOTs disintegrate to vRNPs and tether to the condensed chromosomes. It is speculated that HMGB1 may remodel the chromatin surrounding the vRNPs, which then aid in the tethering of vRNPs. In this study, BUD23-TRMT112 was also found to mediate the tethering of vRNPs. It is speculated that BUD23-TRMT112 may act

directly by an unknown mechanism to BoDV-1 vRNPs via the RdRp domain of BoDV-1 L, or BUD23-TRMT112 may act indirectly via the tertiary structure imposed by the m^7G methylation within the gRNA in BoDV-1 vRNPs.